Coordinate regulation of tissue macrophage and dendritic cell population dynamics by CSF-1

Elisa Tagliani,[1] Chao Shi,[3] Patrice Nancy,[1] Chin-Siean Tay,[1] Eric G. Pamer,[3] and Adrian Erlebacher[1,2]

[1]Department of Pathology and [2]New York University Cancer Institute, New York University School of Medicine, New York, NY 10016
[3]Immunology Program, Sloan-Kettering Institute, Memorial Sloan-Kettering Cancer Center, New York, NY 10065

Tissue macrophages (Mϕs) and dendritic cells (DCs) play essential roles in tissue homeostasis and immunity. How these cells are maintained at their characteristic densities in different tissues has remained unclear. Aided by a novel flow cytometric technique for assessing relative rates of blood-borne precursor recruitment, we examined Mϕ and DC population dynamics in the pregnant mouse uterus, where rapid tissue growth facilitated a dissection of underlying regulatory mechanisms. We demonstrate how Mϕ dynamics, and thus Mϕ tissue densities, are locally controlled by CSF-1, a pleiotropic growth factor whose in situ level of activity varied widely between uterine tissue layers. CSF-1 acted in part by inducing Mϕ proliferation and in part by stimulating the extravasation of Ly6C^{hi} monocytes (Mos) that served as Mϕ precursors. Mo recruitment was dependent on the production of CCR2 chemokine receptor ligands by uterine Mϕs in response to CSF-1. Unexpectedly, a parallel CSF-1–regulated, but CCR2-independent pathway influenced uterine DC tissue densities by controlling local pre-DC extravasation rates. Together, these data provide cellular and molecular insight into the regulation of Mϕ tissue densities under noninflammatory conditions and reveal a central role for CSF-1 in the coordination of Mϕ and DC homeostasis.

CORRESPONDENCE
Adrian Erlebacher:
adrian.erlebacher@nyumc.org

Abbreviations used: Ab, antibody; Mϕ, macrophage; Mo, monocyte; mRNA, messenger RNA; PTX, pertussis toxin.

Macrophages (Mϕs) and DCs are central components of the mononuclear phagocyte system and arise from myeloid progenitor cells residing in the bone marrow (Varol et al., 2009c; Geissmann et al., 2010; Liu and Nussenzweig, 2010). Recently, a great deal of progress has been made concerning the lineage relationships between these progenitors and the circulating precursors they continuously generate. Furthermore, the regulation of DC turnover within secondary lymphoid organs has been substantially clarified by the identification of blood-borne pre-DCs as common precursors to all classical DC subsets (Liu et al., 2009). However, Mϕs and DCs are also abundant throughout all nonlymphoid tissues, and the control of their population dynamics has remained poorly understood. At the cellular level, these peripheral Mϕ and DC pools are thought to be maintained by the continual recruitment of blood-borne precursors and the in situ proliferation of more mature cells (van Furth, 1970; Liu and Nussenzweig, 2010). However, detailed mechanistic experiments have been hampered by the slow turnover of the cells at steady-state and the multiple and diverse effects of the key cytokines and chemokines that control their production and distribution.

The difficulty in studying Mϕ and DC population dynamics in nonlymphoid tissues is exemplified by work on the prototypical Mϕ growth factor colony-stimulating factor 1 (CSF-1 or M-CSF; Pixley and Stanley, 2004). CSF-1 is produced by a variety of stromal and epithelial cell types and signals through the CSF-1R (CD115) tyrosine kinase receptor (encoded by the *Csf1r*/*c-fms* proto-oncogene) expressed by cells of the mononuclear phagocyte lineage (Sasmono et al., 2003). Although an

The Rockefeller University Press $30.00
J. Exp. Med. Vol. 208 No. 9 1901-1916
www.jem.org/cgi/doi/10.1084/jem.20110866

The Journal of Experimental Medicine

overall requirement for CSF-1–CSF-1R interactions in generating tissue Mϕs is clear from the paucity of these cells in CSF-1–deficient (*Csf1*$^{op/op}$) and CSF-1R–deficient (*Csf1r*$^{-/-}$) mice (Wiktor-Jedrzejczak et al., 1990; Dai et al., 2002), the specific contributions of CSF-1–regulated pathways to the control of Mϕ homeostasis remain poorly defined. One site of action is thought to be the bone marrow, where CSF-1 facilitates the production of blood monocytes (Mos) that serve as Mϕ precursors (Pixley and Stanley, 2004). However, systemic CSF-1 injection into *Csf1*$^{op/op}$ mice fails to normalize Mϕ densities in all tissues (Cecchini et al., 1994), and several experimental models have shown that tissue-restricted CSF-1 overexpression increases local Mϕ tissue densities (Moore et al., 1996; Naito et al., 1996; Lin et al., 2001). Together, these results suggest that CSF-1 can act instructively within peripheral tissues themselves. Based upon in vitro data but limited evidence in vivo, such tissue-level effects might include increased Mϕ proliferation or survival (Tushinski et al., 1982; Le Meur et al., 2002b; Jose et al., 2003). It has also been suggested that local CSF-1 expression might increase Mo recruitment from the blood (Lenda et al., 2003), an idea which is superficially consistent with the ability of CSF-1 to induce Mo and Mϕ chemotaxis (Wang et al., 1988; Jones, 2000). However, this possibility lacks direct evidence and conflicts with the notion that Mo extravasation is predominantly a chemokine-driven process.

The role of CSF-1 in DC homeostasis has also remained unclear. Consistent with their greatly reduced abundance in *Csf1r*$^{-/-}$ mice, epidermal Langerhans cells and CX3CR1^{hi} DCs in the gut lamina propria are both thought to be Mo derived (Dai et al., 2002; Ginhoux et al., 2006; Bogunovic et al., 2009; Varol et al., 2009b). In contrast, pre-DCs likely give rise to the CD103^{+} CD11b^{lo} and CD103^{-} CD11b^{hi} DC subsets common to many tissues (Ginhoux et al., 2009). Although no absolute deficits in these two latter subsets have been noted in the absence of CSF-1 signaling, both CD11b^{hi} DCs and pre-DCs express CD115, and *Csfr1*$^{-/-}$ mice show a relative loss of peripheral CD11b^{hi} CD103^{-} DCs as compared with CD11b^{lo} CD103^{+} DCs (Ginhoux et al., 2009; Schmid et al., 2010). It is unclear whether this phenotype is the result of the two subsets having a differential dependence on CSF-1 for in situ proliferation and/or survival or the result of a differential dependence on pre-DC or Mo recruitment from the blood. The pathways that drive pre-DC extravasation into peripheral tissues are also currently unclear, and whether these pathways might be CSF-1 regulated is unknown.

A large body of literature has documented the importance of CSF-1 in controlling Mϕ tissue densities in the mouse uterus (Cohen et al., 1999). Regulation of uterine CSF-1 expression by sex hormones is thought to explain the estrous cycle–related changes in uterine Mϕ densities, and intraluminal CSF-1 injection into the uteri of ovariectomized mice increases uterine Mϕ densities (Pollard et al., 1987; Wood et al., 1992). As with other organ systems, however, the cellular parameters locally regulated by CSF-1 (i.e., proliferation, recruitment, and survival) have remained unclear. For reasons that are also poorly understood, murine pregnancy is associated with dramatic and tissue layer–specific shifts in uterine Mϕ densities (Pollard et al., 1991; Stewart and Mitchell, 1991; Brandon, 1995). Mϕ tissue densities decline dramatically in the decidua, i.e., the specialized and rapidly growing endometrial stromal tissue that directly encases the conceptus but are maintained in the growing segments of myometrial smooth muscle that form the outer portion of each implantation site. Recently, we noted a similar behavior with respect to uterine DCs, which suggested that Mϕs and DCs homeostatically expand in the myometrium but lose density in the decidua through a linked mechanism (Collins et al., 2009). More generally, these observations suggested that the pregnant uterus would provide a robust, yet physiological model system for studying Mϕ and DC population dynamics. To facilitate our analysis, we developed a novel flow cytometric technique that allowed us to directly assess relative rates of Mo and pre-DC extravasation into peripheral tissues.

We show that increased CSF-1 activity within the growing myometrium of pregnant mice drives the homeostatic expansion of Mϕs within this tissue layer. CSF-1 not only directly stimulated the in situ proliferation of myometrial Mϕs but also induced Mϕ precursor recruitment from the blood. These precursors consisted of Ly6C^{hi} Mos, a Mo subset which typically gives rise to Mϕs at sites of inflammation after their recruitment by the set of inflammatory chemokine ligands that engage the CCR2 chemokine receptor (e.g., CCL2/MCP-1; Varol et al., 2009c). Indeed, CCR2 ligands also mediated Ly6C^{hi} Mo extravasation into the growing myometrium, but their localized expression was not caused by an underlying inflammatory process but rather by the select action of CSF-1 itself on myometrial Mϕs. Critically, a parallel CSF-1–driven, but CCR2 ligand–independent pathway induced pre-DC extravasation into the myometrium to promote the expansion of CD11b^{hi} DCs. In addition to explaining the spatial distribution of Mϕs and DCs in the pregnant mouse uterus, these data give fundamental insight into how CSF-1 controls Mϕ tissue densities under non-inflammatory conditions and reveal an intimate, CSF-1–mediated link between tissue Mϕ and DC homeostasis.

RESULTS

Pregnancy entails tissue layer–specific shifts in uterine Mϕ and DC densities

The mouse uterus contains two abundant populations of Mϕs, defined by F4/80^{+} MHCII^{hi} and F4/80^{+} MHCII^{lo} surface phenotypes, as well as many F4/80^{-} MHCII^{hi} CD11c^{hi} DCs with LN-homing capacity that divide into CD11b^{lo} (CD103^{+}) and CD11b^{hi} (CD103^{-}) subsets (Fig. 1 A; Collins et al., 2009). As shown by F4/80 and CD11c immunohistochemistry (Fig. 1 B), these cells were evenly distributed between the myometrium and endometrium at the time of implantation on embryonic day (E) 4.5 but lost tissue density selectively within the decidua upon growth of the implantation site, in accord with prior data (Pollard et al., 1991;

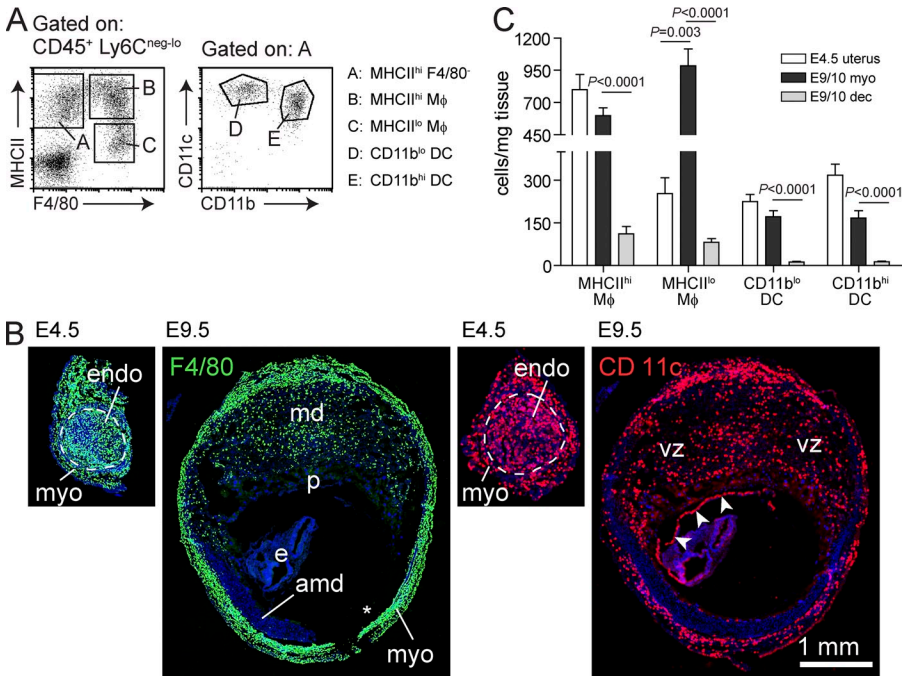

Figure 1. Mϕ and DC tissue densities in the pregnant uterus. (A) Flow cytometric identification of cell populations in uteri of virgin mice. Forward versus side scatter and 7-AAD$^-$ CD45$^+$ Ly6C$^{neg\text{-}lo}$ gating (not depicted) was used to identify all viable leukocytes aside from Ly6C^{hi} Mos and eosinophils. (B) Anti-F4/80 (green) or anti-CD11c (red) immunostaining of transverse sections of E4.5 uteri (unimplanted segments) and an E9.5 implantation site. Dashed lines demarcate the undecidualized endometrium (endo) from the myometrium (myo) on E4.5. The asterisk indicates where part of the antimesometrial decidua (amd) has detached from the slide. The arrowheads indicate nonspecific staining of the yolk sac. DAPI was used as a counterstain. The scale bar applies to all images. Data are representative of at least three independent experiments. e, embryo; md, mesometrial decidua; p, placenta; vz, decidual vascular zone. (C) Flow cytometric assessment of Mϕ and DC tissue densities in the pregnant uterus. Cell suspensions prepared from implantation sites at E9.5/10.5 (E9/10), after physical separation of the myometrium from the decidua (dec) or from the total uterus on E4.5. This latter tissue contains equal amounts of endometrium and myometrium (Collins et al., 2009). n = 4–8 mice per group from four independent experiments. Error bars indicate SEM.

Stewart and Mitchell, 1991; Brandon, 1995; Collins et al., 2009). A similar result was obtained via a flow cytometric analysis of cell suspensions prepared from dissected uterine tissue layers, which allowed us to more accurately identify cell subsets and quantitate their tissue densities (Fig. 1 C). Strikingly, Mϕ and DC densities in the growing segments of myometrium overlying each implantation site at midgestation (i.e., E9.5–10.5) were roughly similar to those seen in the total uterus on E4.5, indicating the rapid homeostatic expansion of the cells within this tissue layer. Importantly, analysis by Annexin V/7-AAD staining argued against a process of selective DC or Mϕ apoptosis in the decidua (unpublished data), and we also previously showed that the decrease in decidual DC density was not caused by DC emigration (Collins et al., 2009).

Myometrial growth is associated with uniquely high extravasation rates of Ly6C^{hi} Mos and pre-DCs

To understand why Mϕ and DC population dynamics differed so dramatically between the myometrium and decidua, we first made note of the prior observation that the decidual vascular zone contains many Mo-like cells adherent to the luminal side of vessel endothelium, even after vascular perfusion, but a relative paucity of leukocytes from the underlying parenchyma (Welsh and Enders, 1985; Kruse et al., 1999). Because many of the vascular adherent cells also express appreciable levels of the DC marker CD11c (Fig. 2, A and B; Behrends et al., 2008), it raised the possibility that Mϕs and DCs failed to expand in the decidua because this tissue layer was not able to induce the extravasation of key cellular precursors. To explore this possibility in more detail, we developed a technique for quantitating, via flow cytometry, the proportion of intravascular versus extravascular leukocytes in a tissue. Analogous to prior work (Galkina et al., 2005; Pereira et al., 2009), this technique involved injecting mice i.v. ≤5 min before sacrifice with a low dose (1 μg/mouse) of fluorochrome-conjugated antibodies (Abs) specific for the pan-leukocyte marker CD45. As expected, this led to 100% of blood leukocytes becoming fluorochrome$^+$ (Fig. 2 C, left). In contrast, cell suspensions prepared from E8.5 uterine tissues and gated on total CD45$^+$ cells showed distinct fluorochrome$^+$ versus fluorochrome$^-$ subpopulations, which we interpreted as being intravascular and extravascular leukocytes, respectively (Fig. 2 C, middle and right). The validity of this interpretation was confirmed by immunofluorescence staining of implantation sites from E8.5 pregnant mice i.v. injected with biotin-conjugated anti-CD45 Abs, which revealed the biotin$^+$ cells exclusively within CD31$^+$ blood vessels (Fig. 2, D and E). Multicolor flow cytometry furthermore allowed us to determine the blood/tissue partitioning of any leukocyte subtype of interest in a given cell suspension. Thus, in the aforementioned experiment (Fig. 2 C), we used CX3CR1^{GFP} reporter mice to identify myeloid cell types such as Mos and Mϕs by virtue of their GFP fluorescence (Geissmann et al., 2003). Strikingly, a much larger proportion of GFP$^+$ cells were in the intravascular compartment in the decidua as compared with the myometrium, which is again consistent with a defect in precursor extravasation.

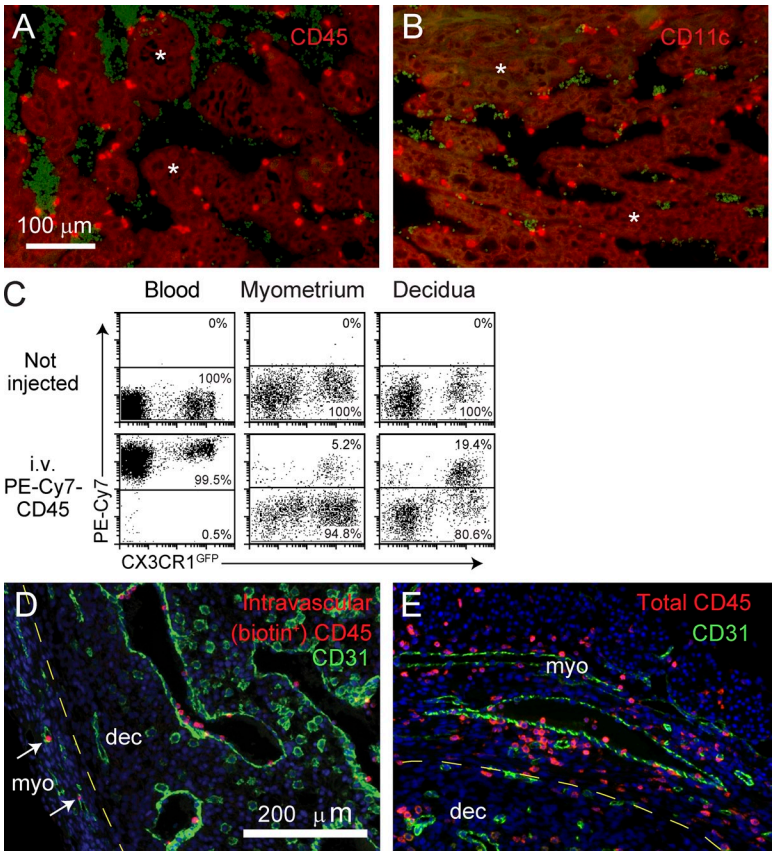

Figure 2. Technique for assessing leukocyte blood/tissue partitioning. (A and B) Leukocyte localization in the decidual vascular zone. Tissue sections from E8.5 implantation sites were stained with anti-CD45 (A) or anti-CD11c (B) Abs (red). Vascular sinusoids are the dark areas containing scattered red blood cells that are green-tinged as a byproduct of the staining protocol. Some areas of the decidual parenchyma are indicated with asterisks. Data are representative of at least $n = 6$ mice from at least six independent experiments. (C) Visualization of leukocyte blood/tissue partitioning in the blood and the E8.5 myometrium and decidua. Pregnant CX3CR1^{GFP} mice were i.v. injected with PE-Cy7–conjugated anti-CD45 Abs 1 min before sacrifice. Total leukocytes in blood and tissue cell preparations were subsequently identified with Pacific orange–conjugated anti-CD45 Abs. Intravascular leukocytes appear as PE-Cy7$^+$, whereas extravascular cells appear as PE-Cy7$^-$. Data are representative of $n = 6$ mice from four independent experiments. (D and E) Histological validation. Tissue sections from E8.5 pregnant mice injected with biotin-conjugated anti-CD45 Abs 5 min before sacrifice were double stained with anti-CD31 Abs (green) and either streptavidin (D; red) or anti-CD45 Abs (E; red). The areas shown are at the border between the myometrium (myo) and mesometrial decidua (dec), where leukocytes are present in the parenchyma of both tissue layers. Note that all biotin$^+$ cells are present within CD31$^+$ vessels, even within the myometrium (left; arrows). Nonvascular CD31$^+$ cells are decidual NK cells. Data are representative of $n = 2$ mice from two independent experiments. DAPI was used as a counterstain.

Next, we used mitotic pulse labeling with the thymidine analogue BrdU (which has an ∼0.5-h half-life in vivo; Packard et al., 1973) as a means to track cohorts of newly generated Ly6C^{hi} Mos and pre-DCs in vivo. Consistent with their intrinsic nonmitotic status (Geissmann et al., 2003), Ly6C^{hi} Mos in blood and uterine tissues showed no BrdU labeling 2 h after a single BrdU injection (Fig. 3 A, top; see Fig. S1 for our Mo and pre-DC gating strategies). In contrast, ∼50% of these cells, representing a synchronous cohort of recent bone marrow emigrants derived from dividing promonocytes (van Furth and Cohn, 1968), showed labeling 24 h after injection (Fig. 3 A, bottom). These labeling kinetics moreover demonstrated that the entire population of uterine Ly6C^{hi} Mos had equilibrated with blood Ly6C^{hi} Mos within 24 h. Similarly, pre-DCs in the blood and peripheral tissues showed minimal labeling (<0.5%) 2 h after BrdU injection (Fig. 3 B, top), but a substantial fraction of the cells became labeled 24 h after injection, including those in the E8.5 myometrium and decidua (Fig. 3 B, bottom). Interestingly, ∼25% of pre-DCs in the bone marrow became labeled with BrdU 2 h after injection (Fig. 3, B and C), and maximal labeling of the cells in peripheral blood (∼50%) was apparent after 12 h (Fig. 3 C), which is consistent with their rapid turnover.

Combining the kinetic dimension provided by BrdU pulse labeling with our technique for discriminating intravascular from extravascular leukocytes allowed us to assess relative rates of Ly6C^{hi} Mo and pre-DC extravasation into different tissues and tissue layers. Strikingly, 24 h after BrdU injection, ∼27–40% of Ly6C^{hi} Mos and pre-DCs in the growing E8.5 myometrium were both BrdU labeled as well as located in the extravascular compartment (i.e., were negative for i.v. injected anti-CD45 Abs; Fig. 4 A). These cells were ones that had, during the 24 h between BrdU injection and sacrifice, completed DNA replication in the bone marrow, transited through the blood to the uterus, and then entered the tissue parenchyma. In contrast, only ∼6–9% of Ly6C^{hi} Mos and pre-DCs were both BrdU$^+$ and extravascular in the decidua. These data thus indicated that the growing myometrium rapidly recruited both Ly6C^{hi} Mos and pre-DCs from the circulation, whereas the extravasation rates of both precursor cell types were much lower in the decidua.

Importantly, the blood/tissue partitionings of the BrdU-labeled cohorts of Ly6C^{hi} Mos and pre-DCs in the myometrium and decidua closely approximated the partitionings of their respective total populations (Fig. 4 B). This implied that measurements of blood/tissue partitionings alone could be used to estimate relative extravasation rates in different organs. Strikingly, Ly6C^{hi} Mos and pre-DCs (when detectable) were both largely (>70%) intravascular in the nonpregnant uterus, lung, kidney, and heart (Fig. 4 C). In the lung, this high degree of intravascular retention indeed reflected the true state of the cells under noninflammatory conditions, as intranasal LPS administration induced many lung Mos to shift to an extravascular location, where they subsequently differentiated into

DC-like cells (Fig. 4 D). In contrast, only the spleen and LN showed the largely extravascular partitioning of Ly6C^{hi} Mos and pre-DCs seen in the growing myometrium (Fig. 4 C), as expected from previous results (Liu et al., 2007; Swirski et al., 2009). Together, these data indicated that the growing myometrium was unique among nonlymphoid tissues in its ability to recruit large numbers of Ly6C^{hi} Mos and pre-DCs from the circulation under noninflammatory conditions. This in turn suggested that high rates of precursor extravasation might be critical for maintaining Mϕ and DC tissue densities.

CCR2 signaling drives Ly6C^{hi} Mo but not pre-DC recruitment to the growing myometrium

Next, we determined the signals that induced Ly6C^{hi} Mo and pre-DC extravasation into the growing myometrium. As shown in Fig. 5 A, i.v. pertussis toxin (PTX) injection shortly before sacrifice on E9.5–10.5 significantly increased the proportion of intravascular Ly6C^{hi} Mos and pre-DCs in the growing myometrium without changing their abundance in the blood (Fig. 5 B). Because PTX inhibits Gαi-mediated G protein–coupled receptor signaling and thus all chemokine receptor signaling, this result suggested that the extravasation of both Ly6C^{hi} Mos and pre-DCs was chemokine driven. Next, we evaluated the role of CCR2, the chemokine receptor which mediates Ly6C^{hi} Mo recruitment to sites of inflammation. Although *Ccr2*$^{-/-}$ mice show substantially reduced numbers of Ly6C^{hi} Mos in the blood and peripheral tissues as a result of their defective exit from the bone marrow (Serbina and Pamer, 2006; Tsou et al., 2007), a clear population of these cells was still visible in uterine cell suspensions. Strikingly, the proportion of these CCR2-deficient cells in the intravascular compartment of the myometrium was greatly increased compared with C57BL/6 (B6) controls (Fig. 5 A), whereas the largely intravascular partitioning of these cells in the decidua remained similar to WT (not depicted). In contrast, pre-DC abundance was normal in the blood of *Ccr2*$^{-/-}$ mice (not depicted), and the blood/tissue partitioning of these cells in the growing myometrium of *Ccr2*$^{-/-}$ mice at midgestation was similar to WT (Fig. 5 A). Myometrial pre-DC blood/tissue partitioning was also unaltered in pregnant mice deficient in CCR1 (unpublished data), a chemokine receptor recently implicated in pre-DC migration to tumors (Diao et al., 2010). Together, these data indicated that Ly6C^{hi} Mo extravasation into the growing myometrium was dependent on CCR2, whereas myometrial pre-DC extravasation, although likely chemokine driven, was independent of CCR1 and CCR2.

Mϕ and DC differentiation in the pregnant uterus

To determine the fate of Ly6C^{hi} Mos in the pregnant uterus, we adoptively transferred Ly6C^{hi} Mos sorted from the bone marrow of CX3CR1$^{GFP/+}$ CD45.1 mice into congenic CD45.2 pregnant recipients. The cells were MHCII^{-} CD11c^{-} F4/80^{-} at the time of transfer on E4.5 (not depicted) and were identified as being GFP^{+} CD45.1^{+} 5–6 d later on E9.5–10.5 (Fig. 6 A, top left). Strikingly, >90% of donor-derived cells in the growing myometrium had entered the extravascular compartment (Fig. 6 A, bottom left, blue cells). A great majority (~90%) of these extravasated cells displayed the

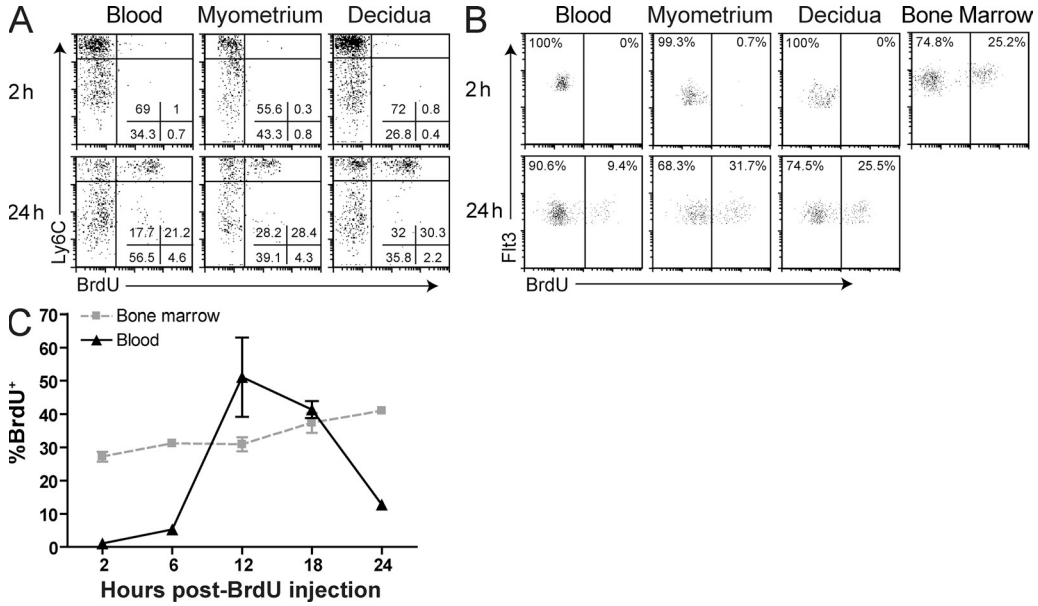

Figure 3. Identification of uterine Ly6C^{hi} Mos and pre-DCs recently arriving from the bone marrow. (A and B) BrdU pulse labeling of Mos (A) and pre-DCs (B). E7.5 (A) or E9.5–10.5 (B) pregnant mice were BrdU injected 2 or 24 h before sacrifice. Data are representative of *n* = 3–5 mice per time point from two and four independent experiments, respectively (A), and *n* = 3–7 mice from three and four independent experiments, respectively (B). (C) Pre-DC BrdU labeling kinetics in the blood and bone marrow. Mice were BrdU injected at the indicated times before sacrifice. *n* = 3–7 mice per group from five independent experiments. Error bars indicate SEM.

F4/80^{+} MHCII$^{lo/hi}$ surface phenotype seen with the endogenous population of uterine Mϕs, whereas only ∼3% of the cells displayed the F4/80^{-} MHCII^{hi} (and CD11b^{hi} CD11c^{hi}; not depicted) surface phenotype of CD11b^{hi} DCs (Fig. 6 A, top right). Similarly, donor-derived cells in the decidua showed a much greater propensity to differentiate into Mϕs upon extravasation (as opposed to DCs; Fig. 6 A, top right); however, most of these cells remained undifferentiated and appeared retained within the intravascular compartment (Fig. 6 A, bottom left and middle right, orange cells). Together, these

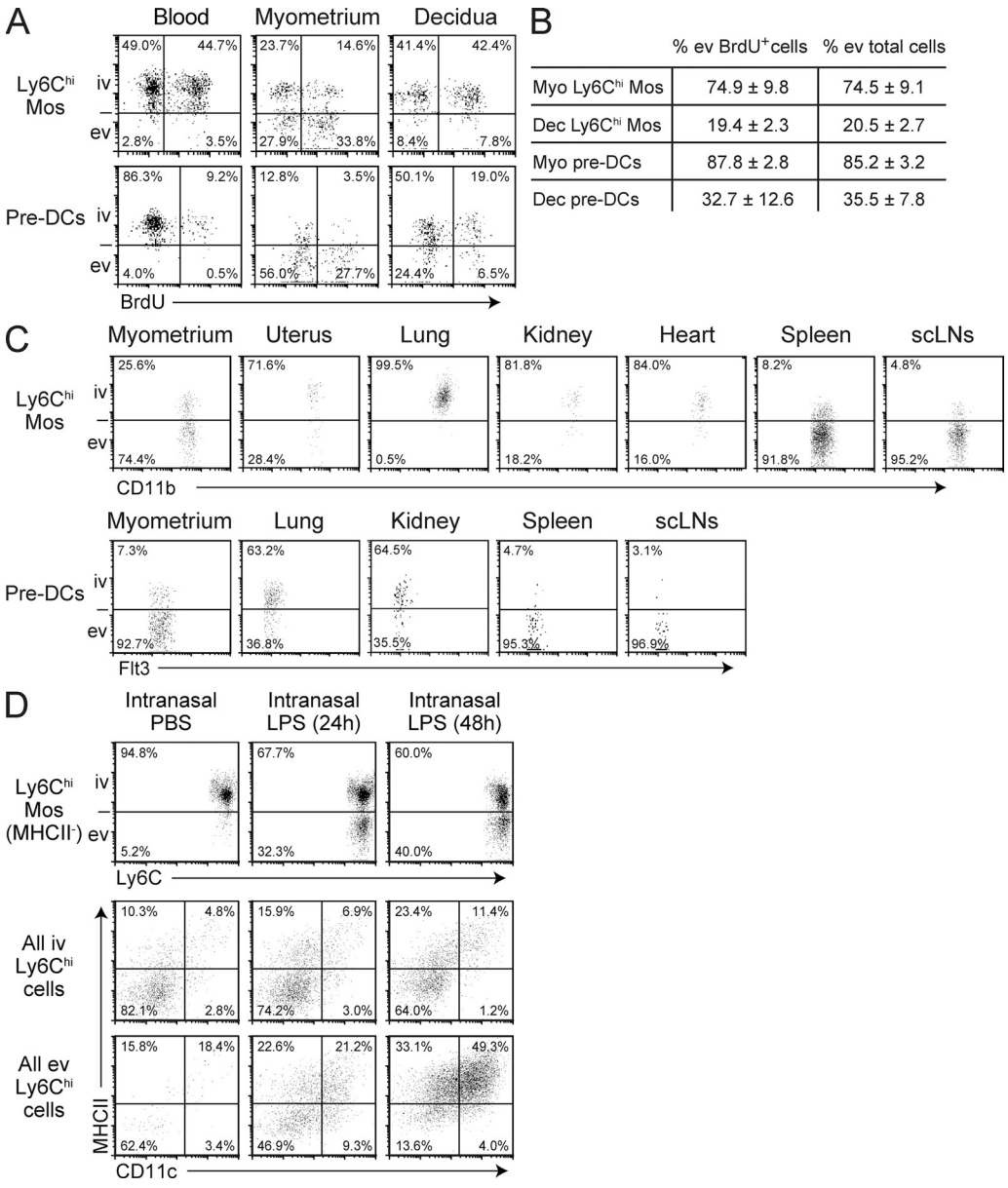

Figure 4. Uniquely high Ly6C^{hi} Mo and pre-DC extravasation rates in the growing myometrium. (A and B) Simultaneous visualization of BrdU labeling and blood/tissue partitioning of Ly6C^{hi} Mos and pre-DCs in the E8.5 pregnant uterus. Mice were injected with BrdU 24 h before sacrifice. Representative dot plots are shown in A; B shows the mean ± SEM percentage of extravascular (ev) cells calculated for either the BrdU-labeled cohort or total population of Ly6C^{hi} Mos or pre-DCs (n = 5–6 mice per group from four and three independent experiments, respectively). Dec, decidua; iv, intravascular; Myo, myometrium. (C) Ly6C^{hi} Mo and pre-DC blood/tissue partitioning in lymphoid and nonlymphoid tissues. The myometrium is from an E9.5 pregnant mouse; the uterus is from a nonpregnant mouse in diestrus. Pre-DCs in the nonpregnant uterus and heart were very scarce and so are not depicted. Data are representative of n = 2–5 mice per group from three and five independent experiments, respectively. scLN, subcutaneous LN. (D) Lung Ly6C^{hi} Mo extravasation and differentiation after the intranasal infusion of PBS or 2 µg LPS. Top panels show the blood/tissue partitioning of Ly6C^{hi} Mos. The CD11c/MHCII surface phenotype of all Ly6C^{hi} cells is shown in the middle and bottom panels, which are gated on intravascular and extravascular cells, respectively. All plots were generated from the same number of CD45^{+} cells and thus reveal the relative proportions of the displayed cells in different mice. Data are representative of n = 2 mice per group from three independent experiments.

data suggested that Ly6C^{hi} Mos were almost exclusively Mϕ precursors in the pregnant uterus but robustly differentiated only if they could enter the uterine parenchyma.

Given our reliance on the CX3CR1^{GFP} marker to accurately identify donor-derived cells, the aforementioned experiment did not allow us to assess the contribution of Ly6C^{hi} Mos to CD11b^{lo} DCs, which are CX3CR1^{-} (Jakubzick et al., 2008). Thus, we also made use of mice deficient in Flt3L, a growth factor required for the generation of all DC subsets (McKenna et al., 2000). Indeed, the uteri of nonpregnant *Flt3L*$^{-/-}$ mice showed >90% reductions in the tissue densities of both CD11b^{lo} and CD11b^{hi} DC subsets as compared with WT controls (unpublished data). Strikingly, *Flt3L*$^{-/-}$ mice at midgestation also showed dramatically reduced densities of both DC subsets in the growing myometrium (∼87% and ∼70%, respectively; Fig. 6 B) as well as dramatic reductions in the abundance of pre-DCs in the blood (Fig. 6 C).

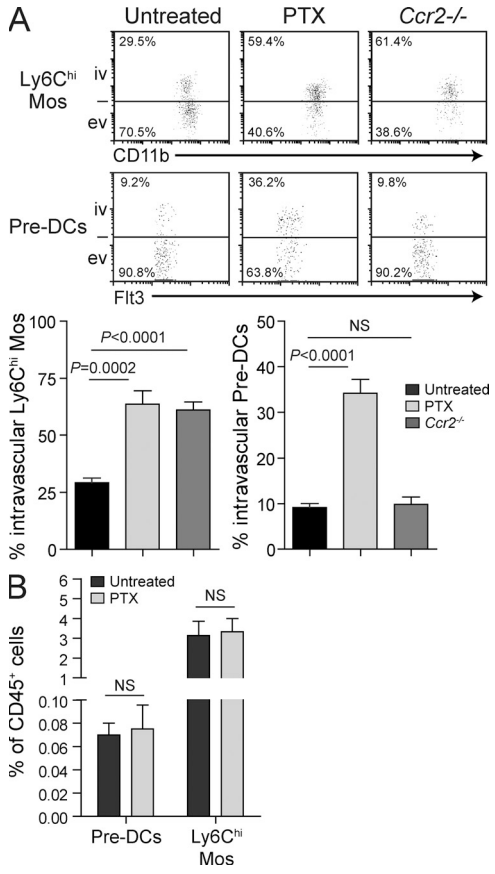

Figure 5. PTX sensitivity and CCR2 dependence of precursor recruitment to the myometrium. (A) Blood/tissue partitioning of Ly6C^{hi} Mos (top) and pre-DCs (bottom) in the E9.5–10.5 growing myometrium of untreated WT mice, WT mice injected i.v. with 0.5 µg PTX 16 h and 15 min before sacrifice, or untreated *Ccr2*$^{-/-}$ mice. Data are from two to five independent experiments with n = 4–8 mice per group. ev, extravascular; iv, intravascular. (B) Effect of PTX treatment on blood Ly6C^{hi} Mo and pre-DC abundance. E9.5–10.5 pregnant mice were injected with PBS or 0.5 µg PTX 16 h and 15 min before sacrifice. n = 2–4 mice per group from three independent experiments. Error bars indicate SEM.

In contrast, these mice showed no detectable change in myometrial Mϕ tissue densities or blood Ly6C^{hi} Mo abundance (Fig. 6, B and C). Thus, we conclude that pre-DCs constitute the vast majority of precursors for both DC subsets in the growing myometrium.

CSF-1–dependent and –independent proliferative responses of Mϕs and DCs in the pregnant uterus

We next measured short-term (2 h) BrdU incorporation rates to assess the contribution of in situ proliferation to uterine Mϕ and DC population dynamics. As shown in Fig. 7 A, MHCII^{hi} and MHCII^{lo} Mϕs showed very low levels of BrdU incorporation in the nonpregnant uterus (<1%) and relatively low levels in the E4.5 uterus and the E9.5–10.5 decidua (∼1–5%). In contrast, both Mϕ subsets were highly proliferative in the growing myometrium (∼10% BrdU^{+}). This phenotype was potentially caused by the elevation in uterine CSF-1 expression known to occur during pregnancy (Arceci et al., 1989). Indeed, using PCR primers that detect all known *Csf1* messenger RNA (mRNA) isoforms, we found that *Csf1* mRNA levels in the growing myometrium were 18-, 11-, and 49-fold higher than the nonpregnant uterus, E4.5 uterus, and decidua, respectively, and ∼5–30-fold higher than all other tissues tested (Fig. 7 B). More importantly, the injection of anti–CSF-1R blocking Abs 12 h before sacrifice dramatically reduced the BrdU labeling of both subsets of Mϕs in the myometrium without affecting their labeling in the decidua (Fig. 7 C). This result indicated that elevated CSF-1 activity in the myometrium was directly responsible for the in situ proliferation of myometrial Mϕs.

Next, we examined DC proliferation. BrdU labeling indices of both CD11b^{lo} and CD11b^{hi} DCs were similar in the nonpregnant and E4.5 uterus (∼4–9%). However, by midgestation, the labeling of CD11b^{lo} DCs increased to ∼15% and ∼12% in the myometrium and decidua, respectively (Fig. 7 D, left), whereas the labeling of CD11b^{hi} DCs remained constant in the myometrium but declined to ∼2% in the decidua (Fig. 7 D, right). Myometrial CD11b^{hi} DCs were the only DC population that showed reduced proliferation after acute CSF-1R blockade (Fig. 7 E), whereas CD11b^{lo} DCs appeared more sensitive to loss of Flt3L (Fig. 7 F). Nonetheless, myometrial CD11b^{lo} DCs in pregnant *Flt3L*$^{-/-}$ mice still showed substantially elevated proliferation as compared with nonpregnant controls (Fig. 7, compare F with D; P = 0.001). Together, these results indicated that uterine growth after implantation was associated with an induction of myometrial CD11b^{lo} DC in situ proliferation, primarily through the actions of an Flt3L- and CSF-1–independent mitogen, and a decrease in decidual CD11b^{hi} DC in situ proliferation.

CSF-1 stimulates Ly6C^{hi} Mo extravasation into the myometrium by inducing CCR2 ligand expression by myometrial Mϕs

Along with its inhibitory effect on Mϕ proliferation, the injection of anti–CSF-1R Abs 12 h before sacrifice on E9.5–10.5 unexpectedly increased the proportion of intravascular

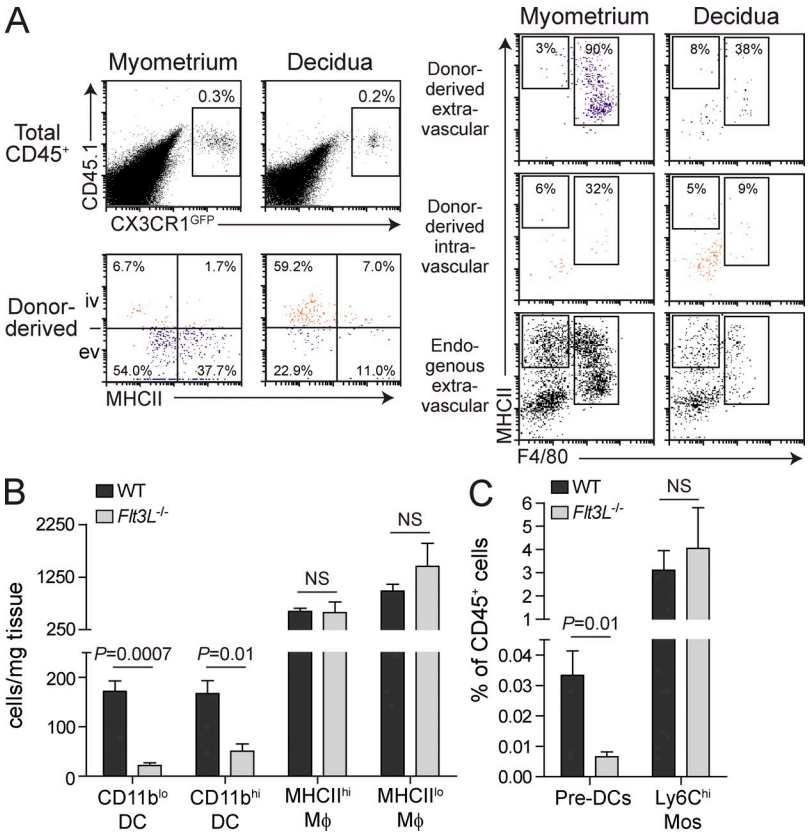

Figure 6. Origin of uterine Mϕs and DCs. (A) Fate of adoptively transferred Ly6C^{hi} Mos. Pregnant CD45.2 mice on E4.5 were injected with Ly6C^{hi} bone marrow Mos from CD45.1 CX3CR1^{GFP} donors. 5 or 6 d later, donor cells were identified as being CD45.1$^+$ GFP$^+$ (top left) before visualization of their blood/tissue partitioning and MHCII expression status (bottom left). The percentage of extravascular (ev; blue) or intravascular (iv; orange) donor-derived cells in each tissue layer that had become Mϕs or CD11b^{hi} DCs is shown within the two gated populations in the top right and middle right plots. The bottom right plots show the surface phenotype of the endogenous population of extravasated leukocytes (i.e., CD45$^+$ cells that are negative for i.v. anti-CD45) in each tissue layer. Data are representative of $n = 4$ mice from two independent experiments. (B) Mϕ and DC tissue densities in the E9.5–10.5 myometrium of *Flt3L*$^{-/-}$ pregnant mice. $n = 4$–8 mice per group from six independent experiments. (C) Pre-DC and Ly6C^{hi} Mo abundances in the blood of *Flt3L*$^{-/-}$ mice. $n = 3$–7 mice per group from six independent experiments. Error bars indicate SEM.

Ly6C^{hi} Mos in the growing myometrium to ∼40% as compared with the 25% seen in isotype control–treated mice (Fig. 8 A). A similar shift in the blood/tissue partitioning of myometrial Ly6C^{hi} Mos was also seen in mice treated for a consecutive 3-d period with anti–CSF-1R Abs starting on E6.5–7.5 (Fig. 8 A). CSF-1R blockade did not affect the abundance of Ly6C^{hi} Mos in the blood (Fig. 8 B) or the blood/tissue partitioning of Ly6C^{hi} Mos in the decidua (not depicted). Together, these results indicated that CSF-1 contributed to the elevated rates of Ly6C^{hi} Mo extravasation within the growing myometrium. However, because Mo extravasation was also CCR2 dependent (Fig. 5 A), we tested whether CSF-1 was acting indirectly through the induction of CCR2 ligands. Indeed, the myometrium showed approximately three- to eightfold higher *Ccl2*, *Ccl7*, and *Ccl12* mRNA levels as compared with the decidua, and these levels were dramatically reduced in the myometrium but not decidua after short-term CSF-1R blockade (Fig. 8 C). Moreover, both flow cytometric and immunohistochemical assessments of MCP1-RFP reporter mice revealed that almost all CCL2$^+$ cells in the growing myometrium were F4/80$^+$ Mϕs (Fig. 8 D). Together, these data indicated that the high rate of Ly6C^{hi} Mo extravasation into the growing myometrium depended on elevated in situ levels of CSF-1 activity that in turn induced the expression of CCR2 ligands by myometrial Mϕs.

Role of CSF-1 in uterine Mϕ maturation and phenotypes

We next determined the effect of CSF-1R blockade on uterine Mϕ densities. In the nonpregnant uterus, where CSF-1 mRNA levels are low (Fig. 7 B), Mϕs are not proliferating (Fig. 7 A), and there is minimal recruitment of circulating Ly6C^{hi} Mos (not depicted; Collins et al., 2009), treatment with anti–CSF-1R Abs for a consecutive 3-d period led to almost a complete loss of both MHCII^{hi} and MHCII^{lo} Mϕs (Fig. 9 A). This result is in accord with recent data (MacDonald et al., 2010) and indicated that basal levels of CSF-1R signaling are required for the survival of uterine Mϕs. In contrast, mice treated for 3 d with anti–CSF-1R Abs starting on E6.5–7.5 still retained relatively large numbers of MHCII^{hi} Mϕs in the growing myometrium (Fig. 9 A; representative dot plots shown in Fig. 9 B, top). This result suggested that Ab-mediated CSF-1R blockade was not complete in the growing myometrium on E9.5–10.5, where CSF-1 activity is high, and that the survival of MHCII^{hi} Mϕs might be less dependent on CSF-1R signaling than the survival of MHCII^{lo} Mϕs. Alternatively, it was possible that CSF-1 had an additional function in maintaining newly differentiating Mϕs as cells with a MHCII^{lo} surface phenotype, as suggested by previous in vitro data (Calamai et al., 1982; Willman et al., 1989). In this case, the effects of CSF-1R blockade would include the conversion of MHCII^{lo} Mϕs to MHCII^{hi} Mϕs.

Use of *Ccr2*$^{-/-}$ mice allowed us to discriminate between these alternatives. Nonpregnant *Ccr2*$^{-/-}$ mice showed reduced uterine Mϕ densities compared with WT (Fig. 9 C). Furthermore, the E9.5–10.5 growing myometrium showed an ∼70% reduction in MHCII^{hi} Mϕ densities (Fig. 9 C), even though the proliferation rates of both MHCII^{hi} and MHCII^{lo} myometrial Mϕs were unaltered in *Ccr2*$^{-/-}$ mice compared with WT (not depicted). These results demonstrated that the

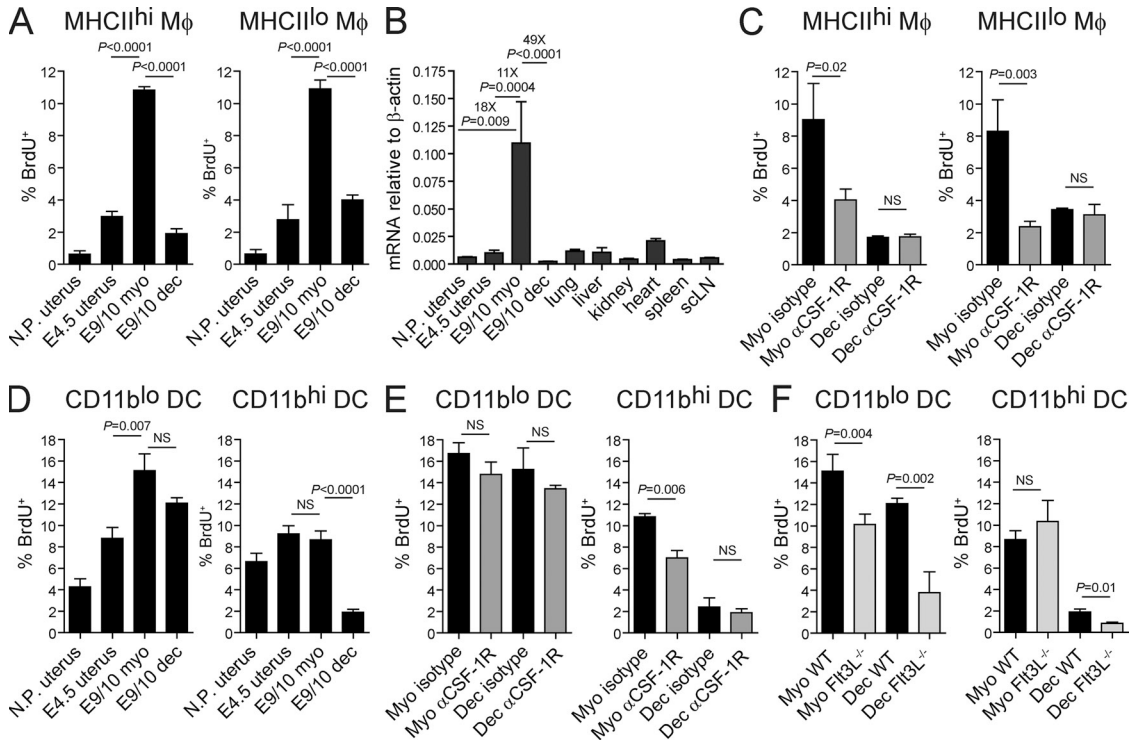

Figure 7. Mϕ and DC in situ proliferation in the pregnant and nonpregnant uterus. BrdU incorporation was measured by flow cytometry 2 h after injection. Uterine cell suspensions were prepared from uteri of nonpregnant mice (N.P. uterus), from pregnant uteri on E4.5 (E4.5 uterus), and from the myometrium (myo) and decidua (dec) on E9.5–10.5 (E9/10). (A and D) Proliferation of uterine Mϕs (A) and DCs (D) in B6 mice. $n = 4–6$ mice per group from six independent experiments. (B) Quantitative RT-PCR assessment of *Csf1* mRNA expression levels in various lymphoid and nonlymphoid organs. scLN, subcutaneous LN. $n = 2–8$ mice per group from at least two independent experiments. (C and E) Proliferation of uterine Mϕs (C) and DCs (E) after CSF-1R blockade. E9.5–10.5 pregnant mice were injected with anti–CSF-1R or isotype control Abs 12 h before sacrifice. $n = 3–6$ mice per group from five independent experiments. (F) Uterine DC proliferation in pregnant *Flt3L*$^{-/-}$ mice. $n = 4–5$ mice per group from four independent experiments. Error bars indicate SEM.

overall maintenance of uterine Mϕ densities was critically dependent on CCR2. Unexpectedly, however, *Ccr2*$^{-/-}$ mice showed normal MHCII^{lo} myometrial Mϕ densities at midgestation (Fig. 9 C). This observation could be explained if we hypothesized, as in the previous paragraph, that CSF-1 inhibited Mϕ maturation in addition to inducing Mϕ in situ proliferation. Thus, we determined how a single injection of anti–CSF-1R blocking Abs into pregnant *Ccr2*$^{-/-}$ mice would affect the relative densities of MHCII^{lo} and MHCII^{hi} Mϕs in the myometrium 48 h later on E9.5–10.5. Indeed, this treatment reduced the density of MHCII^{lo} Mϕs but actually increased the density of MHCII^{hi} Mϕs, indicating the conversion of MHCII^{lo} to MHCII^{hi} cells (Fig. 9 C; representative dot plots shown in Fig. 9 B, bottom).

Thus, in addition to driving Mϕ expansion through the dual induction of Mϕ in situ proliferation and CCR2 ligand expression, CSF-1 activity in the growing myometrium inhibited Mϕ maturation and thus promoted the relative accumulation of MHCII^{lo} cells. Interestingly, as compared with MHCII^{hi} Mϕs from the same samples, MHCII^{lo} Mϕs sorted from the myometrium at midgestation expressed significantly higher mRNA levels of *Lyve1*, a marker associated with angiogenic Mϕs (Fig. 9 D; Cho et al., 2007). These cells also expressed higher levels of genes indicative of the alternatively activated (or M2) phenotype associated with tissue remodeling and repair, including *Cd163*, *Stab1* (stabilin-1), and *Mrc1* (mannose receptor). In contrast, the MHCII^{hi} Mϕs showed a trend toward higher expression levels of *Ccl5*, *Cx3cl1*, and *Ccl17*, which encode chemokines expressed more by M1 Mϕs (Movahedi et al., 2010; unpublished data). Together, these data suggested that the program of CSF-1–induced Mϕ expansion in the myometrium inherently ensured the presence of adequate numbers of Mϕs potentially specialized for the demands of tissue growth.

CSF-1 influences DC tissue densities in the growing myometrium by regulating the extravasation of their precursors from the blood

Unexpectedly, we also found that acute CSF-1R blockade affected the blood/tissue partitioning of pre-DCs in the growing myometrium. Thus, injection of anti–CSF-1R Abs 12 h before sacrifice on E9.5–10.5 increased the proportion of intravascular pre-DCs to ∼23% as compared with the ∼10% seen in isotype control–treated mice (Fig. 10 A). A similar shift was observed in

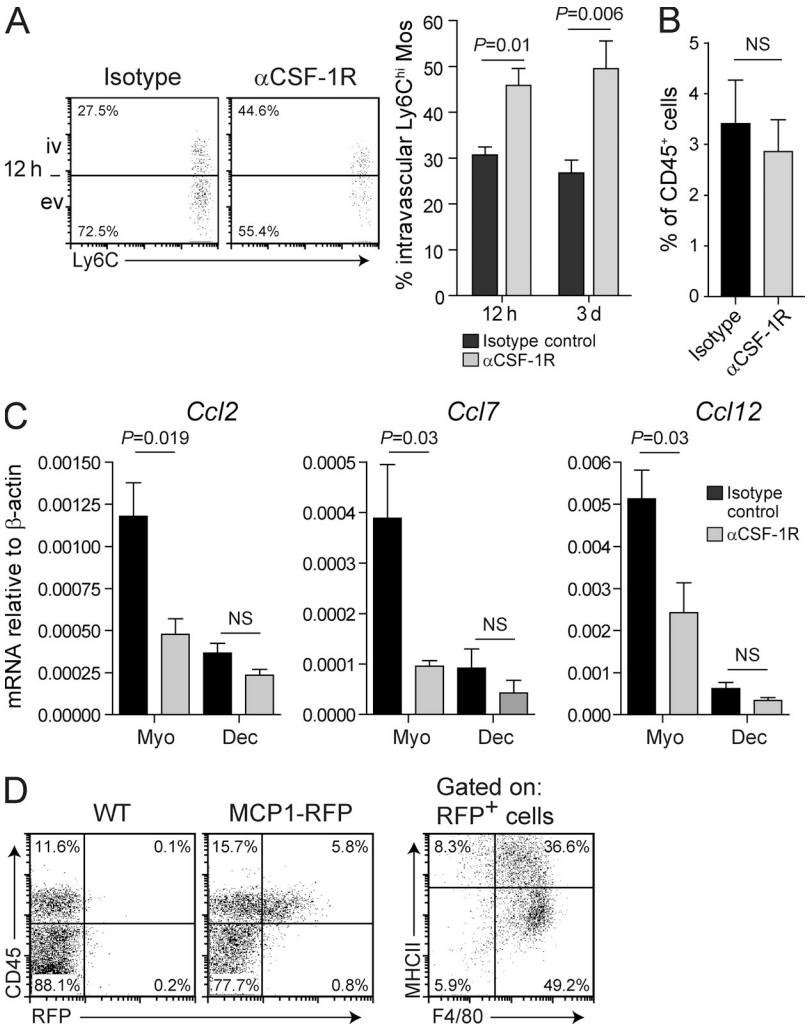

Figure 8. Mϕs promote the extravasation of circulating Ly6C^{hi} Mos into the growing myometrium through their CSF-1–induced expression of CCR2 ligands. (A–C) Mice were injected with anti–CSF-1R or isotype control Abs 12 h (A and C) or 3 d consecutively before sacrifice on E9.5–10.5 (A and B). (A) Blood/tissue partitioning of Ly6C^{hi} Mos in the myometrium. Representative dot plots from the 12-h time point are shown on the left; graph data are from n = 5–9 mice per group from six independent experiments. ev, extravascular; iv, intravascular. (B) Blood Ly6C^{hi} Mo abundance. n = 4–5 mice per group from three independent experiments. (C) Effect of acute CSF-1R blockade on uterine CCR2 ligand mRNA expression. *Ccl2*, *Ccl7*, and *Ccl12* mRNA levels were measured by quantitative RT-PCR analysis of whole tissue. Mice were injected with Abs 12 h before sacrifice. n = 4 mice per group compiled over three independent experiments. Error bars indicate SEM. dec, decidua; myo, myometrium. (D) Analysis of CCL2 expression in myometrium cell suspensions using E9.5–10.5 pregnant MCP1-RFP reporter mice. Data are representative of n = 3 MCP1-RFP reporter mice and n = 2 pregnant WT mice from one experiment; similar results were obtained by tissue immunostaining in an independent experiment (n = 3 mice; not depicted).

mice treated with anti–CSF-1R Abs for a consecutive 3-d period starting on E6.5–7.5 (Fig. 10 A) and was not associated with any change in pre-DC abundance in the blood or bone marrow (Fig. 10 B). Together, these data indicated that CSF-1R blockade decreased pre-DC extravasation rates in the growing myometrium.

We next determined the effect of CSF-1R blockade on DC tissue densities. Strikingly, mice given anti–CSF-1R Abs for a consecutive 3 d starting on E6.5–7.5 showed an ∼45% reduction in myometrial CD11b^{hi} DCs densities as compared with isotype control–treated mice (Fig. 10 C) and a mild 15% but statistically insignificant reduction in myometrial CD11b^{lo} DC densities. For CD11b^{hi} DCs, reduced myometrial tissue densities could only in part be explained by the effect of CSF-1R blockade on in situ proliferation rates, as this effect was relatively small (a decrease in BrdU labeling from ∼11 to 7%; Fig. 7 E). Moreover, control experiments performed on nonpregnant mice showed that uterine DC tissue densities were unaffected by 3 d of CSF-1R blockade, indicating that the anti–CSF-1R Ab did not induce DC emigration or death (Fig. 10 D). Indeed, CSF-1R blockade also had no major effect on DC densities in the decidua (Fig. 10 C), where CSF-1 activity levels and pre-DC extravasation rates are both low. Together, these data suggested that CSF-1–induced pre-DC extravasation into the E6.5–9.5 myometrium was critical for maintaining DC tissue densities during this period of massive DC homeostatic expansion.

DISCUSSION

We have studied Mϕ and DC population dynamics in the mouse uterus during the first half of gestation, when the implanted uterus grows ∼15-fold in 8 d. Most clearly, our results provide a framework for understanding how local Mϕ tissue densities are specified by in situ levels of CSF-1 activity (Fig. S2 A). In the E9.5–10.5 myometrium overlying each implantation site, we found that high levels of CSF-1 activity drive the proliferation of resident Mϕs as well as their expression of the CCR2 ligands CCL2, CCL7, and CCL12. These chemokines in turn recruit blood-borne Ly6C^{hi} Mos, which differentiate into additional Mϕs. Thus, Mϕs within the growing myometrium undergo a homeostatic expansion through two interlocking CSF-1–driven mechanisms, and Mϕ tissue densities remain relatively constant. In contrast, the decidua shows relatively low levels of CSF-1 activity associated with low rates of Mϕ proliferation, low levels of CCR2 ligand expression, and the low rates of Ly6C^{hi} Mo extravasation typical of most peripheral tissues. Thus, decidual Mϕs do

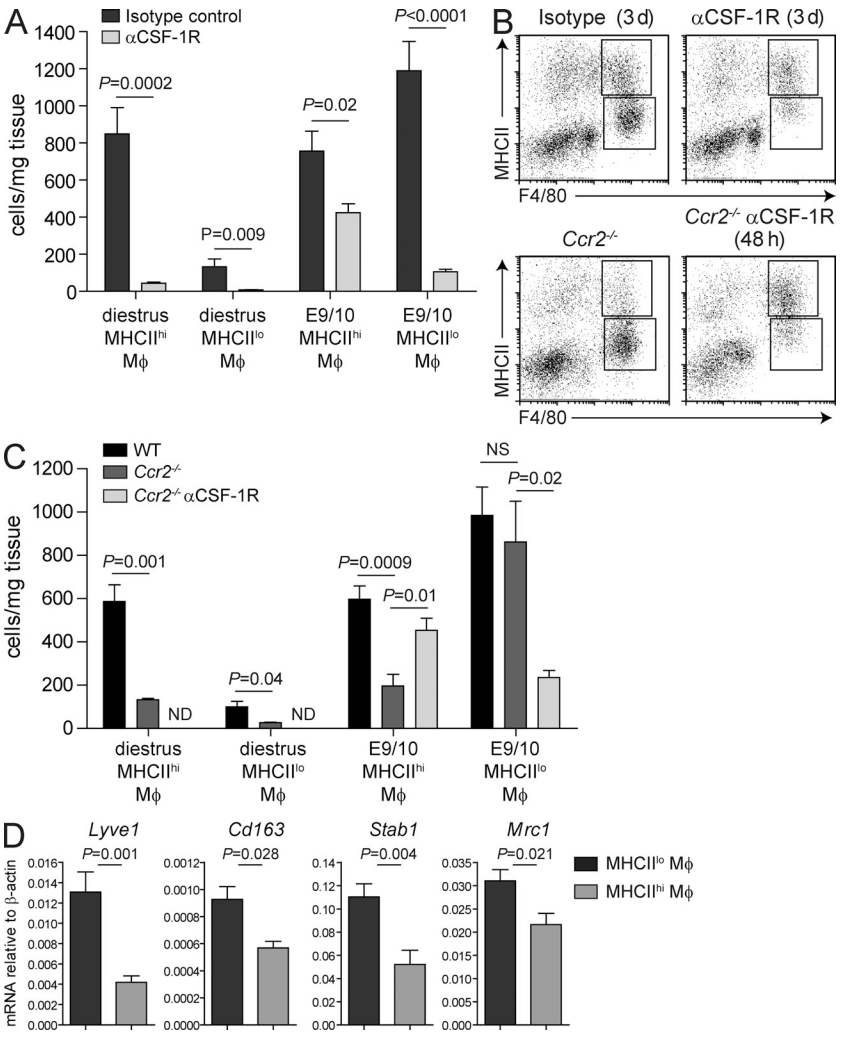

Figure 9. Effect of CSF-1R blockade and CCR2 deficiency on uterine Mϕ densities and differentiation. Uterine cell suspensions were prepared from nonpregnant mice in diestrus or from the E9.5–10.5 myometrium. (A) Effect of CSF-1R blockade on uterine Mϕ densities. Mice were injected with anti–CSF-1R or isotype control Abs for the consecutive 3 d before sacrifice. n = 6–8 mice per group from two (nonpregnant) or six (pregnant) independent experiments. (B) Representative dot plots of myometrial CD45+ cells showing MHCIIhi and MHCIIlo Mϕs (top and bottom boxes, respectively) in the pregnant WT mice contributing to the data shown in A (top) or the pregnant *Ccr2*$^{-/-}$ mice contributing to the data shown in C (bottom). (C) Uterine Mϕ densities in nonpregnant and pregnant *Ccr2*$^{-/-}$ mice. Some mice were also injected i.v. once with anti–CSF-1R Abs 48 h before sacrifice. n = 4–8 mice per group from two (nonpregnant), six (pregnant), or two (48-h CSF-1R blockade) independent experiments. (D) Expression profiles of MHCIIlo and MHCIIhi Mϕs in the E9.5–10.5 growing myometrium. Mϕ subsets were sorted from enzymatically dispersed tissues and subjected to qRT-PCR analysis. n = 3–7 mice from at least four independent experiments. Error bars indicate SEM.

not expand to match the growth of the tissue, and decidual Mϕ densities decline.

Importantly, our principal evidence for the myometrium and decidua containing high and low levels of CSF-1 activity, respectively, comes from a functional evaluation of the effect of CSF-1R blockade on Mϕ in situ proliferation rates. Thus, CSF-1R blockade inhibited the high rate of Mϕ proliferation seen in the myometrium but had no discernable effect on the low rate of Mϕ proliferation seen in the decidua. We also found that the E9.5–10.5 myometrium expressed much higher *Csf1* mRNA levels than the nonpregnant and E4.5 uterus and the E9.5–10.5 decidua, as well as all other peripheral tissues tested. This observation is consistent with the presence of scattered CSF-1–expressing cells in the myometrium of pregnant CSF-1–lacZ reporter mice (Ryan et al., 2001) and suggests that high CSF-1 activity in this tissue layer was in part caused by local *Csf1* transcriptional induction. However, it is important to note that CSF-1 bioavailability is under multiple additional levels of regulation, including the generation of different biologically active protein isoforms, local production versus acquisition from the blood, extracellular matrix sequestration, and receptor-mediated ligand scavenging (Pixley and Stanley, 2004). How these other levels of regulation influence in situ CSF-1 activity within the pregnant uterus is currently unclear. Indeed, ligand scavenging by decidual stromal cells and trophoblasts, which are some of the few adult cell types to express CSF-1R aside from mononuclear phagocytes, might be particularly important for maintaining low CSF-1 activity levels in the decidua given the mild increase in serum CSF-1 levels during pregnancy and the abundant epithelial expression of *Csf1* mRNA in the segments of uterus between implantation sites (Bartocci et al., 1986; Arceci et al., 1989; Regenstreif and Rossant, 1989).

Although our detailed analysis of Mϕ population dynamics was rendered feasible by the unique growth properties of the pregnant uterus, the core aspects of our model (Fig. S2 A) are consistent with isolated pieces of data from several different systems, which suggests its potential broad relevance. For example, CSF-1 is a well-known Mϕ mitogen in vitro (Pixley and Stanley, 2004), and several studies have implicated its up-regulated expression as a cause of increased Mϕ proliferation in the context of inflammation (Isbel et al., 2001; Le Meur et al., 2002a,b; Jose et al., 2003). Similarly, our failure to detect a significant contribution of apoptosis to the loss of decidual Mϕ density is not only consistent with the relatively similar levels of *Csf1* mRNA expression in the decidua and nonpregnant uterus, but also with older data indicating that much lower concentrations of CSF-1 are needed to maintain Mϕ viability than are needed to induce Mϕ proliferation (Tushinski et al., 1982). Thus, as inferred from our experiments

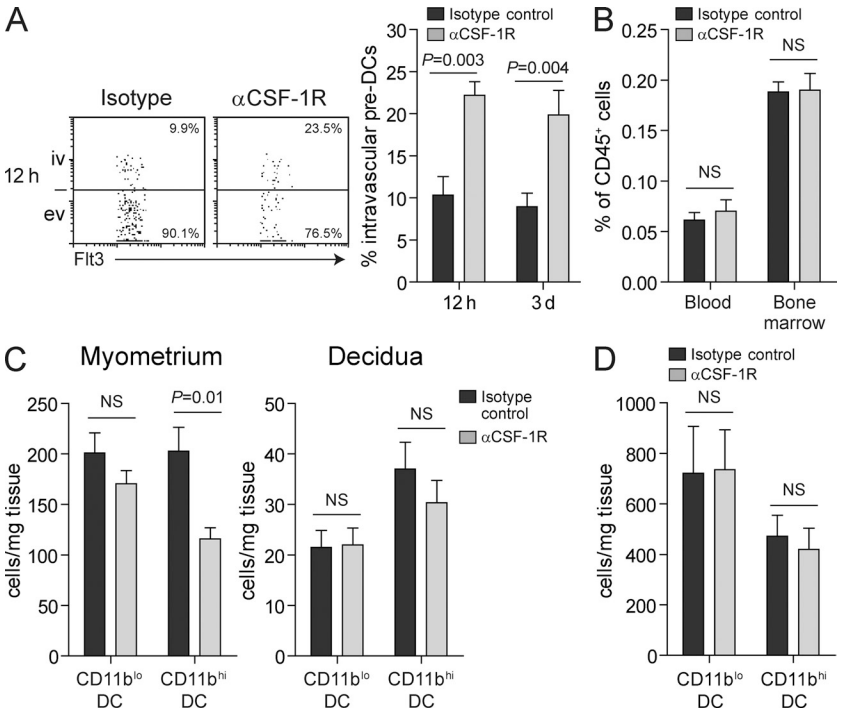

Figure 10. CSF-1 influences uterine pre-DC extravasation rates and DC densities. (A–C) Mice were injected with anti–CSF-1R or isotype control Abs 12 h (A) or 3 d consecutively before sacrifice on E9.5–10.5 (A–C). (A) Blood/tissue partitioning of pre-DCs in the myometrium. Representative dot plots from the 12-h time point are shown on the left; $n = 3$–8 mice per group from four and five independent experiments, respectively. ev, extravascular; iv, intravascular. (B) Pre-DC abundance in the blood and bone marrow. $n = 5$–8 mice per group from three independent experiments. (C) Uterine DC tissue densities. $n = 6$–8 mice per group from six independent experiments. (D) DC tissue densities in the nonpregnant uterus after 3 d of CSF-1R blockade. $n = 6$ mice per group from two independent experiments. Error bars indicate SEM.

on the nonpregnant uterus, apoptosis may only be a feature of Mϕ population dynamics in the pregnant uterus when mice are treated with CSF-1R blocking Abs.

Perhaps most significantly, CSF-1 has recently been shown to directly induce CCR2 ligand expression by Mϕs in vitro (Baran et al., 2007; Irvine et al., 2009; El Chartouni et al., 2010). This result explains the inflammation-associated correlations between CSF-1 expression and local CCL2 levels noted in vivo (Guleria and Pollard, 2001; Baran et al., 2007), as well as suggestions of CSF-1–mediated Mo recruitment (Lenda et al., 2003) without a need to invoke a direct chemotactic role for CSF-1 in leukocyte extravasation. However, our demonstration that CSF-1–regulated myometrial Mϕs express physiologically relevant levels of CCR2 ligands in the absence of inflammation suggests that these chemokines might be more broadly important for regulating peripheral tissue Mo/Mϕ homeostasis than previously appreciated. Discerning this role has previously been difficult because the abundance of Ly6C^{hi} Mos in the blood of *Ccr2*$^{-/-}$ mice is severely reduced at baseline as a result of their impaired exit from the bone marrow (Serbina and Pamer, 2006; Tsou et al., 2007). It will be of particular interest to evaluate whether CSF-1 in the tumor microenvironment induces Mo extravasation through effects on CCR2 ligand expression, as this would predict that combined use of CSF-1R and CCR2 antagonists would synergistically reduce tumor-associated Mϕ abundance.

Our data also provide significant insight into the tissue layer–specific regulation of DC densities in the pregnant uterus. Previously, we showed that loss of DC density in the decidua was not caused by DC emigration from this tissue layer (Collins et al., 2009), and our current data find little evidence for the selective apoptosis of decidual DCs. Rather, the divergence in DC densities between the myometrium and decidua was attributable to a low rate of decidual CD11b^{hi} DC in situ proliferation and, with relevance to both DC subsets, to a major difference in DC precursor recruitment from the blood. In the case of CD11b^{lo} DCs, these precursors were pre-DCs; in the case of CD11b^{hi} DCs, they were pre-DCs and to a very limited extent Ly6C^{hi} Mos. Growth of the entire implantation site was also associated with a CSF-1–independent and largely Flt3L-independent increase in CD11b^{lo} DC in situ proliferation rates, suggesting that there is a previously unrecognized mitogen for this subset that can be produced by peripheral tissues under certain circumstances. Although clearly insufficient to maintain the tissue density of CD11b^{lo} DCs in the decidua, it was likely that in situ proliferation contributed to the homeostatic expansion of this DC subset in the myometrium. In contrast, CD11b^{hi} DCs in the midgestation myometrium showed no change in proliferation rates as compared with the E4.5 uterus, suggesting that the growth-induced expansion of this subset relied primarily on precursor recruitment.

As with Ly6C^{hi} Mos, we surprisingly found that myometrial pre-DC extravasation rates were reduced upon CSF-1R blockade. Because pre-DCs express CSF-1R (Schmid et al., 2010; unpublished data), it is formally possible that this effect reflects an ability of CSF-1 to act as a direct pre-DC chemoattractant. However, in separate experiments, we found that myometrial pre-DC extravasation was inhibited by PTX, which implies that the relevant chemotactic receptor is Gαi coupled, unlike CSF-1R, and thus likely a chemokine receptor. Thus, it is more likely that CSF-1R induces pre-DC extravasation because it induces expression of a pre-DC–attracting chemokine by a cell type already present within the myometrium. Substantiating the existence of this novel pathway will require identifying the relevant pre-DC chemoattractant and the CSF-1–responding cell type; however, it is striking that it

forms such a direct parallel with the CSF-1–mediated induction of CCR2 ligands by myometrial Mϕs that drives Ly6C^{hi} Mo extravasation (Fig. S2 B). CSF-1–induced pre-DC extravasation, whether as a direct or indirect effect, helps explain our finding that 3 d of CSF-1R blockade reduced CD11b^{hi} DC densities in the growing myometrium, a finding which could only in part be ascribed to the reduction in CD11b^{hi} DC proliferation after CSF-1R blockade. Indeed, the select effect of CSF-1R blockade on CD11b^{hi} DC densities may be more the consequence of our aforementioned inference that CD11b^{hi} DC expansion is more dependent on precursor extravasation than CD11b^{lo} DC expansion. This inference may also explain the recent observation that *Csf1*$^{op/op}$ mice show a relative loss of CD11b^{hi} DCs compared with CD11b^{lo} DCs in a variety of peripheral tissues (Ginhoux et al., 2009). However, the fact that the absolute DC tissue density defects in *Csf1*$^{op/op}$ mice are not nearly as severe as their Mϕ tissue density defects demonstrates that pre-DC extravasation is also mediated in part by non–CSF-1–dependent pathways.

Together, these data place CSF-1 at the top of a regulatory hierarchy that couples Mϕ and DC population dynamics in peripheral tissues through the linked regulation of Mo and pre-DC extravasation rates. By virtue of the differences in the levels of CSF-1 activity between uterine tissue layers, this regulatory mechanism is exploited in the postimplantation mouse uterus to coordinate the homeostatic expansion of Mϕs and DCs in the growing myometrium and their decrease in density in the decidua. Previously, we argued that the decreased density of decidual DCs, in combination with their physical entrapment within the tissue, prevents the initiation of immunogenic T cell responses to the fetus and placenta (Collins et al., 2009). Presumably, the parallel reduction in decidual Mϕ density in the mouse either has its own physiological significance or is a byproduct of a critical need to reduce DC densities at the maternal/fetal interface. Provocatively, immunohistochemical analyses of placental bed biopsies from third trimester pregnant women have suggested that both Mϕs and DCs are more abundant in the deciduae of patients with preeclampsia (Lockwood et al., 2006; Huang et al., 2008; Schonkeren et al., 2011), an important obstetrical complication associated with inadequate trophoblast invasion into the uterus and impaired uterine vascular remodeling. In addition, multiple studies have demonstrated elevated serum CSF-1 protein levels in preeclamptic patients (Hayashi et al., 1996, 2003). Although these data are controversial (Keith et al., 2000; Bürk et al., 2001; Redline, 2001; Bersinger and Ødegård, 2005; Kim et al., 2007) and do not imply causal relationships, they raise the possibility that the CSF-1–coupled regulation of Mϕ and DC population dynamics in the decidua may have functional implications for human reproductive health.

In contrast to the decidua, where there is a potentially unique requirement for low Mϕ and DC densities, the CSF-1–coupled maintenance of relatively high Mϕ and DC densities in the growing myometrium might be considered inherently beneficial given the multifaceted roles of these cells in tissue homeostasis and host defense. Indeed, we speculate that the pathways described here might contribute to the maintenance of Mϕ and DC densities in different nonuterine tissues and tissue layers during tissue growth and in the adult organism. Surprisingly, however, Mϕ depletion after 3 d of CSF-1R blockade had no effect on myometrial wet weights (unpublished data), and older work has demonstrated that *Csf1*$^{op/op}$ females carry litters with normal fetal and placental weights (Pollard et al., 1991). Additionally, *Flt3L*$^{-/-}$ females, which are severely deficient in uterine DCs, show no obvious fertility defects (unpublished data). However, this latter result needs to be reconciled with the recent observation that uterine DCs contribute to embryo implantation and early decidualization potentially through effects on decidual vascularization (Krey et al., 2008; Plaks et al., 2008). Indeed, *Csf1*$^{op/op}$ females show modestly elevated embryo resorption rates (Pollard et al., 1991), and our data here indicate that high CSF-1 activity in the growing myometrium, through its inhibitory effect on Mϕ maturation, induces the accumulation of MHCII^{lo} Mϕs with a more M2-like phenotype. Together, these results suggest that CSF-1–regulated uterine Mϕs and DCs may perform a variety of subtle and potentially gestation stage–dependent roles in myometrial and decidual growth and function.

MATERIALS AND METHODS

Mice. B6 (CD45.2) mice were purchased from Taconic or Harlan Laboratories. B6.SJL-*Ptprc*^{a}/BoyAiTac (B6 CD45.1), *Ccr2*$^{-/-}$ (Kuziel et al., 1997), and *Flt3L*$^{-/-}$ (McKenna et al., 2000) mice were purchased from Taconic. CX3CR1$^{GFP/GFP}$ mice (Jung et al., 2000) were a gift of D. Littman (New York University, New York, NY) and were crossed to B6 CD45.1 to generate the CX3CR1$^{GFP/+}$ CD45.1^{+} mice used as Mo donors. MCP1-RFP mice have been described previously (Shi et al., 2011) and bear an RFP expression cassette knocked into the *Ccl2* locus. The aforementioned mice were all on a B6 background, and B6 mice were used as WT mice in all experiments except for the one shown in Fig. 2 (A and B), in which we used B6CBAF1/J mice (The Jackson Laboratory), and the one in Fig. 4 (A and B), in which we pooled data from B6 and B6CBAF1 mice because these data were indistinguishable. Mice were maintained in a specific pathogen–free facility, and all experiments were approved by the New York University School of Medicine Institutional Animal Care and Use Committee. All nonpregnant mice were virgin females treated with progesterone to induce a diestrus-like state. All mating experiments used virgin females and B6 males; noon of day of the appearance of a copulation plug was counted as E0.5.

Flow cytometry and determination of tissue densities and BrdU incorporation rates. Cell suspensions of nonperfused whole uteri or dissected uterine tissue layers were prepared by enzymatic digestion as previously described (Collins et al., 2009). A similar protocol was used to prepare cells from other lymphoid and nonlymphoid tissues. Cells were pretreated with the FcγR-blocking mAb 2.4G2. All analyses were performed using a 10-color LSRII flow cytometer (BD) and FCS Express software (De Novo Software), except for the analysis of MCP1-RFP reporter mice, for which we used an LSRFortessa cytometer (BD). After forward versus side scatter gating to exclude debris, viable leukocytes were identified using the nucleic acid dye 7-AAD (BD) and Pacific orange–conjugated anti-CD45 Abs (clone 30-F11; Invitrogen). The cells were then subtyped using fluorochrome- or biotin-conjugated Abs specific to mouse MHCII (M5/114.15.2), Ly-6C (AL21, HK1.4), F4/80 (BM8, C1:A3-1), CD11c (N418), CD11b (M1/70), Gr-1 (RB6-8C5), B220 (RA3-6B2), CD3 (17A2), CD19 (1D3), NK1.1 (PK138), Ter-119, SIRP-α (P84), CD135 (A2F10), CD45.1 (A20), and CD115

(AFS98) purchased from BD, BioLegend, eBioscience, or AbD Serotec. Tissue layer–specific leukocyte densities in the uterus were determined by weighing dissected tissues before their enzymatic dispersal. Total viable cell numbers were then determined using a hemocytometer with trypan blue exclusion, allowing calculation of total viable cells per milligram of tissue. Multiplying this value with the percent representation of a cell subset of interest gave that subset's density in the units of cells/milligram of tissue. BrdU incorporation rates were determined by staining the cells with FITC-conjugated mouse anti-BrdU Abs (BD) according to the manufacturer's instructions after the cells were first surface stained to identify leukocyte subsets. Mice were injected i.v. with 2 mg BrdU (Sigma-Aldrich) in PBS 2 or 24 h before sacrifice.

Determination of leukocyte blood/tissue partitionings. Mice were i.v. injected 1 or 5 min before sacrifice with 1 µg rat anti-CD45 Abs (30-F11; eBioscience) plus 5 USP units heparin in 100 µl PBS. The Abs were conjugated to PE-Cy7, PerCP-Cy5.5, APC-Cy7, or biotin. At 1 min before sacrifice, anti-CD45 Ab injection led to the labeling of all peripheral blood leukocytes (Fig. 2 C). For convenience, however, we routinely injected the Ab 5 min before sacrifice. Peripheral blood Ly6C^{hi} Mos and pre-DCs remained labeled after this period of time, but other leukocyte subsets began losing the label. Notably, the labeling of splenic Ly6C^{hi} Mos and pre-DCs remained relatively constant at 5 min, 30 min, and 1 h after injection, suggesting that the labeling of these cells becomes saturated by 5 min.

Cell sorting and Ly6C^{hi} Mo adoptive transfer. Sorting was performed on a MoFlo cell sorter (Dako). Bone marrow mononuclear cells from CX3CR1^{GFP} CD45.1 mice were enriched by granulocyte and erythrocyte depletion on a Ficoll density gradient as described previously (Varol et al., 2009a), and 3×10^6 sorted Ly6C^{hi} Mos (GFP$^+$ CD11b$^+$ Ly6C^{hi} CD115^{hi} cells) were i.v. injected into unconditioned pregnant recipient mice. Their contribution to uterine leukocyte populations was assessed 5–6 d later.

Progesterone, PTX, and anti–CSF-1R Ab administration. To induce a diestrus-like state in nonpregnant mice, we subcutaneously injected 2 mg progesterone in 0.1 ml sesame seed oil daily for a consecutive 3 d and sacrificed the mice for analysis 1 d after the last injection. This dosing schedule applied to all experiments with nonpregnant mice except for the ones in which we treated mice additionally for 3 d with anti–CSF-1R Abs. In this case, we gave progesterone for 3 d before the first Ab injection and then continued the progesterone injections during the course of Ab treatment. 0.5 µg PTX (EMD) was injected i.v. in PBS 16 h and 15 min before sacrifice; rat anti–CSF-1R Abs (300 µg per injection; clone AFS98; Sudo et al., 1995) or isotype control Abs (clone 2A3, rat IgG2a), both prepared by BioXCell, were injected i.v. in PBS 12 h, 48 h, or for a consecutive 3 d before sacrifice. The AFS98 hybridoma was supplied by S.-I. Nishikawa (RIKEN Center for Developmental Biology, Chuo-ku, Kobe, Japan).

Immunohistochemistry and quantitative RT-PCR. These methods are described in the Supplemental materials and methods.

Statistical analysis. Results were analyzed with Prism 4.0 (GraphPad Software). All comparisons, except the one for Fig. 7 B for which we used a nonparametric Mann-Whitney test, were performed using a two-tailed Student's *t* test. A p-value <0.05 was taken as statistically significant. All graphs show mean ± SEM.

Online supplemental material. Fig. S1 shows the gating strategies used to identify Mos and pre-DCs. Fig. S2 shows our model of CSF-1–controlled Mϕ and DC population dynamics. Supplemental materials and methods describe our immunohistochemistry and quantitative RT-PCR protocols. Online supplemental material is available at http://www.jem.org/cgi/content/full/jem.20110866/DC1.

We thank S.-I. Nishikawa for the AFS98 hybridoma, which was sent to us by E.R. Stanley (Albert Einstein College of Medicine, Bronx, NY), and J. Ernst and A. Blaisdell for critical review of the manuscript. The Histopathology and Flow Cytometry core facilities of the New York University Cancer Institute provided histological and cell sorting services and were supported by a grant from the National Institutes of Health (NIH) National Cancer Institute (P30CA016087).

This work was supported by grants from the NIH (RO1AI062980) and the American Cancer Society (RSG-10-158-01-LIB) to A. Erlebacher.

The authors declare no financial conflicts of interest.

Author contributions: E. Tagliani and C.-S. Tay performed experiments, P. Nancy provided key reagents, and C. Shi and E.G. Pamer provided MCP1-RFP mice. E. Tagliani and A. Erlebacher designed experiments, analyzed data, and wrote the manuscript.

Submitted: 2 May 2011
Accepted: 19 July 2011

REFERENCES

Arceci, R.J., F. Shanahan, E.R. Stanley, and J.W. Pollard. 1989. Temporal expression and location of colony-stimulating factor 1 (CSF-1) and its receptor in the female reproductive tract are consistent with CSF-1-regulated placental development. *Proc. Natl. Acad. Sci. USA*. 86:8818–8822. doi:10.1073/pnas.86.22.8818

Baran, C.P., J.M. Opalek, S. McMaken, C.A. Newland, J.M. O'Brien Jr., M.G. Hunter, B.D. Bringardner, M.M. Monick, D.R. Brigstock, P.C. Stromberg, et al. 2007. Important roles for macrophage colony-stimulating factor, CC chemokine ligand 2, and mononuclear phagocytes in the pathogenesis of pulmonary fibrosis. *Am. J. Respir. Crit. Care Med.* 176:78–89. doi:10.1164/rccm.200609-1279OC

Bartocci, A., J.W. Pollard, and E.R. Stanley. 1986. Regulation of colony-stimulating factor 1 during pregnancy. *J. Exp. Med.* 164:956–961. doi:10.1084/jem.164.3.956

Behrends, J., C.M. Karsten, S. Wilke, A. Röbke, and A. Kruse. 2008. Identification of ITGA4/ITGB7 and ITGAE/ITGB7 expressing subsets of decidual dendritic-like cells within distinct microdomains of the pregnant mouse uterus. *Biol. Reprod.* 79:624–632. doi:10.1095/biolreprod.107.067041

Bersinger, N.A., and R.A. Ødegård. 2005. Serum levels of macrophage colony stimulating, vascular endothelial, and placenta growth factor in relation to later clinical onset of pre-eclampsia and a small-for-gestational age birth. *Am. J. Reprod. Immunol.* 54:77–83. doi:10.1111/j.1600-0897.2005.00290.x

Bogunovic, M., F. Ginhoux, J. Helft, L. Shang, D. Hashimoto, M. Greter, K. Liu, C. Jakubzick, M.A. Ingersoll, M. Leboeuf, et al. 2009. Origin of the lamina propria dendritic cell network. *Immunity*. 31:513–525. doi:10.1016/j.immuni.2009.08.010

Brandon, J.M. 1995. Macrophage distribution in decidual tissue from early implantation to the periparturient period in mice as defined by the macrophage differentiation antigens F4/80, macrosialin and the type 3 complement receptor. *J. Reprod. Fertil.* 103:9–16. doi:10.1530/jrf.0.1030009

Bürk, M.R., C. Troeger, R. Brinkhaus, W. Holzgreve, and S. Hahn. 2001. Severely reduced presence of tissue macrophages in the basal plate of preeclamptic placentae. *Placenta*. 22:309–316. doi:10.1053/plac.2001.0624

Calamai, E.G., D.I. Beller, and E.R. Unanue. 1982. Regulation of macrophage populations. IV. Modulation of Ia expression in bone marrow-derived macrophages. *J. Immunol.* 128:1692–1694.

Cecchini, M.G., M.G. Dominguez, S. Mocci, A. Wetterwald, R. Felix, H. Fleisch, O. Chisholm, W. Hofstetter, J.W. Pollard, and E.R. Stanley. 1994. Role of colony stimulating factor-1 in the establishment and regulation of tissue macrophages during postnatal development of the mouse. *Development*. 120:1357–1372.

Cho, C.H., Y.J. Koh, J. Han, H.K. Sung, H. Jong Lee, T. Morisada, R.A. Schwendener, R.A. Brekken, G. Kang, Y. Oike, et al. 2007. Angiogenic role of LYVE-1-positive macrophages in adipose tissue. *Circ. Res.* 100:e47–e57. doi:10.1161/01.RES.0000259564.92792.93

Cohen, P.E., K. Nishimura, L. Zhu, and J.W. Pollard. 1999. Macrophages: important accessory cells for reproductive function. *J. Leukoc. Biol.* 66:765–772.

Collins, M.K., C.S. Tay, and A. Erlebacher. 2009. Dendritic cell entrapment within the pregnant uterus inhibits immune surveillance of the maternal/fetal interface in mice. *J. Clin. Invest.* 119:2062–2073.

Dai, X.M., G.R. Ryan, A.J. Hapel, M.G. Dominguez, R.G. Russell, S. Kapp, V. Sylvestre, and E.R. Stanley. 2002. Targeted disruption of the mouse colony-stimulating factor 1 receptor gene results in osteopetrosis, mononuclear phagocyte deficiency, increased primitive progenitor cell frequencies, and reproductive defects. *Blood*. 99:111–120. doi:10.1182/blood.V99.1.111

Diao, J., J. Zhao, E. Winter, and M.S. Cattral. 2010. Recruitment and differentiation of conventional dendritic cell precursors in tumors. *J. Immunol.* 184:1261–1267. doi:10.4049/jimmunol.0903050

El Chartouni, C., C. Benner, M. Eigner, M. Lichtinger, and M. Rehli. 2010. Transcriptional effects of colony-stimulating factor-1 in mouse macrophages. *Immunobiology*. 215:466–474. doi:10.1016/j.imbio.2009.08.002

Galkina, E., J. Thatte, V. Dabak, M.B. Williams, K. Ley, and T.J. Braciale. 2005. Preferential migration of effector CD8+ T cells into the interstitium of the normal lung. *J. Clin. Invest.* 115:3473–3483. doi:10.1172/JCI24482

Geissmann, F., S. Jung, and D.R. Littman. 2003. Blood monocytes consist of two principal subsets with distinct migratory properties. *Immunity*. 19:71–82. doi:10.1016/S1074-7613(03)00174-2

Geissmann, F., M.G. Manz, S. Jung, M.H. Sieweke, M. Merad, and K. Ley. 2010. Development of monocytes, macrophages, and dendritic cells. *Science*. 327:656–661. doi:10.1126/science.1178331

Ginhoux, F., F. Tacke, V. Angeli, M. Bogunovic, M. Loubeau, X.M. Dai, E.R. Stanley, G.J. Randolph, and M. Merad. 2006. Langerhans cells arise from monocytes in vivo. *Nat. Immunol.* 7:265–273. doi:10.1038/ni1307

Ginhoux, F., K. Liu, J. Helft, M. Bogunovic, M. Greter, D. Hashimoto, J. Price, N. Yin, J. Bromberg, S.A. Lira, et al. 2009. The origin and development of nonlymphoid tissue $CD103^+$ DCs. *J. Exp. Med.* 206:3115–3130. doi:10.1084/jem.20091756

Guleria, I., and J.W. Pollard. 2001. Aberrant macrophage and neutrophil population dynamics and impaired Th1 response to *Listeria monocytogenes* in colony-stimulating factor 1-deficient mice. *Infect. Immun.* 69:1795–1807. doi:10.1128/IAI.69.3.1795-1807.2001

Hayashi, M., M. Numaguchi, H. Watabe, and Y. Yaoi. 1996. High blood levels of macrophage colony-stimulating factor in preeclampsia. *Blood*. 88:4426–4428.

Hayashi, M., T. Ohkura, and N. Inaba. 2003. Elevation of serum macrophage colony-stimulating factor before the clinical manifestations of preeclampsia. *Am. J. Obstet. Gynecol.* 189:1356–1360. doi:10.1067/S0002-9378(03)00674-4

Huang, S.J., C.P. Chen, F. Schatz, M. Rahman, V.M. Abrahams, and C.J. Lockwood. 2008. Pre-eclampsia is associated with dendritic cell recruitment into the uterine decidua. *J. Pathol.* 214:328–336. doi:10.1002/path.2257

Irvine, K.M., M.R. Andrews, M.A. Fernandez-Rojo, K. Schroder, C.J. Burns, S. Su, A.F. Wilks, R.G. Parton, D.A. Hume, and M.J. Sweet. 2009. Colony-stimulating factor-1 (CSF-1) delivers a proatherogenic signal to human macrophages. *J. Leukoc. Biol.* 85:278–288. doi:10.1189/jlb.0808497

Isbel, N.M., D.J. Nikolic-Paterson, P.A. Hill, J. Dowling, and R.C. Atkins. 2001. Local macrophage proliferation correlates with increased renal M-CSF expression in human glomerulonephritis. *Nephrol. Dial. Transplant.* 16:1638–1647. doi:10.1093/ndt/16.8.1638

Jakubzick, C., F. Tacke, F. Ginhoux, A.J. Wagers, N. van Rooijen, M. Mack, M. Merad, and G.J. Randolph. 2008. Blood monocyte subsets differentially give rise to CD103+ and CD103− pulmonary dendritic cell populations. *J. Immunol.* 180:3019–3027.

Jones, G.E. 2000. Cellular signaling in macrophage migration and chemotaxis. *J. Leukoc. Biol.* 68:593–602.

Jose, M.D., Y. Le Meur, R.C. Atkins, and S.J. Chadban. 2003. Blockade of macrophage colony-stimulating factor reduces macrophage proliferation and accumulation in renal allograft rejection. *Am. J. Transplant.* 3:294–300. doi:10.1034/j.1600-6143.2003.00068.x

Jung, S., J. Aliberti, P. Graemmel, M.J. Sunshine, G.W. Kreutzberg, A. Sher, and D.R. Littman. 2000. Analysis of fractalkine receptor CX(3)CR1 function by targeted deletion and green fluorescent protein reporter gene insertion. *Mol. Cell. Biol.* 20:4106–4114. doi:10.1128/MCB.20.11.4106-4114.2000

Keith, J.C. Jr., R. Pijnenborg, C. Luyten, B. Spitz, R. Schaub, and F.A. Van Assche. 2000. Maternal serum levels of macrophage colony-stimulating factor are associated with adverse pregnancy outcome. *Eur. J. Obstet. Gynecol. Reprod. Biol.* 89:19–25. doi:10.1016/S0301-2115(99)00154-2

Kim, J.S., R. Romero, E. Cushenberry, Y.M. Kim, O. Erez, J.K. Nien, B.H. Yoon, J. Espinoza, and C.J. Kim. 2007. Distribution of CD14+ and CD68+ macrophages in the placental bed and basal plate of women with preeclampsia and preterm labor. *Placenta*. 28:571–576. doi:10.1016/j.placenta.2006.07.007

Krey, G., P. Frank, V. Shaikly, G. Barrientos, R. Cordo-Russo, F. Ringel, P. Moschansky, I.V. Chernukhin, M. Metodiev, N. Fernández, et al. 2008. In vivo dendritic cell depletion reduces breeding efficiency, affecting implantation and early placental development in mice. *J. Mol. Med.* 86:999–1011. doi:10.1007/s00109-008-0379-2

Kruse, A., M.J. Merchant, R. Hallmann, and E.C. Butcher. 1999. Evidence of specialized leukocyte-vascular homing interactions at the maternal/fetal interface. *Eur. J. Immunol.* 29:1116–1126. doi:10.1002/(SICI)1521-4141(199904)29:04<1116::AID-IMMU1116>3.0.CO;2-4

Kuziel, W.A., S.J. Morgan, T.C. Dawson, S. Griffin, O. Smithies, K. Ley, and N. Maeda. 1997. Severe reduction in leukocyte adhesion and monocyte extravasation in mice deficient in CC chemokine receptor 2. *Proc. Natl. Acad. Sci. USA*. 94:12053–12058. doi:10.1073/pnas.94.22.12053

Le Meur, Y., M.D. Jose, W. Mu, R.C. Atkins, and S.J. Chadban. 2002a. Macrophage colony-stimulating factor expression and macrophage accumulation in renal allograft rejection. *Transplantation*. 73:1318–1324. doi:10.1097/00007890-200204270-00022

Le Meur, Y., G.H. Tesch, P.A. Hill, W. Mu, R. Foti, D.J. Nikolic-Paterson, and R.C. Atkins. 2002b. Macrophage accumulation at a site of renal inflammation is dependent on the M-CSF/c-fms pathway. *J. Leukoc. Biol.* 72:530–537.

Lenda, D.M., E. Kikawada, E.R. Stanley, and V.R. Kelley. 2003. Reduced macrophage recruitment, proliferation, and activation in colony-stimulating factor-1-deficient mice results in decreased tubular apoptosis during renal inflammation. *J. Immunol.* 170:3254–3262.

Lin, E.Y., A.V. Nguyen, R.G. Russell, and J.W. Pollard. 2001. Colony-stimulating factor 1 promotes progression of mammary tumors to malignancy. *J. Exp. Med.* 193:727–740. doi:10.1084/jem.193.6.727

Liu, K., and M.C. Nussenzweig. 2010. Origin and development of dendritic cells. *Immunol. Rev.* 234:45–54. doi:10.1111/j.0105-2896.2009.00879.x

Liu, K., C. Waskow, X. Liu, K. Yao, J. Hoh, and M. Nussenzweig. 2007. Origin of dendritic cells in peripheral lymphoid organs of mice. *Nat. Immunol.* 8:578–583. doi:10.1038/ni1462

Liu, K., G.D. Victora, T.A. Schwickert, P. Guermonprez, M.M. Meredith, K. Yao, F.F. Chu, G.J. Randolph, A.Y. Rudensky, and M. Nussenzweig. 2009. In vivo analysis of dendritic cell development and homeostasis. *Science*. 324:392–397. doi:10.1126/science.1171243

Lockwood, C.J., P. Matta, G. Krikun, L.A. Koopman, R. Masch, P. Toti, F. Arcuri, S.T. Huang, E.F. Funai, and F. Schatz. 2006. Regulation of monocyte chemoattractant protein-1 expression by tumor necrosis factor-alpha and interleukin-1beta in first trimester human decidual cells: implications for preeclampsia. *Am. J. Pathol.* 168:445–452. doi:10.2353/ajpath.2006.050082

MacDonald, K.P., J.S. Palmer, S. Cronau, E. Seppanen, S. Olver, N.C. Raffelt, R. Kuns, A.R. Pettit, A. Clouston, B. Wainwright, et al. 2010. An antibody against the colony-stimulating factor 1 receptor depletes the resident subset of monocytes and tissue- and tumor-associated macrophages but does not inhibit inflammation. *Blood*. 116:3955–3963. doi:10.1182/blood-2010-02-266296

McKenna, H.J., K.L. Stocking, R.E. Miller, K. Brasel, T. De Smedt, E. Maraskovsky, C.R. Maliszewski, D.H. Lynch, J. Smith, B. Pulendran, et al. 2000. Mice lacking flt3 ligand have deficient hematopoiesis affecting hematopoietic progenitor cells, dendritic cells, and natural killer cells. *Blood*. 95:3489–3497.

Moore, K.J., T. Naito, C. Martin, and V.R. Kelley. 1996. Enhanced response of macrophages to CSF-1 in autoimmune mice: a gene transfer strategy. *J. Immunol.* 157:433–440.

Movahedi, K., D. Laoui, C. Gysemans, M. Baeten, G. Stangé, J. Van den Bossche, M. Mack, D. Pipeleers, P. In't Veld, P. De Baetselier, and J.A. Van Ginderachter. 2010. Different tumor microenvironments contain

functionally distinct subsets of macrophages derived from Ly6C(high) monocytes. *Cancer Res.* 70:5728–5739. doi:10.1158/0008-5472.CAN-09-4672

Naito, T., H. Yokoyama, K.J. Moore, G. Dranoff, R.C. Mulligan, and V.R. Kelley. 1996. Macrophage growth factors introduced into the kidney initiate renal injury. *Mol. Med.* 2:297–312.

Packard, D.S. Jr., R.A. Menzies, and R.G. Skalko. 1973. Incorporation of thymidine and its analogue, bromodeoxyuridine, into embryos and maternal tissues of the mouse. *Differentiation.* 1:397–404. doi:10.1111/j.1432-0436.1973.tb00137.x

Pereira, J.P., J. An, Y. Xu, Y. Huang, and J.G. Cyster. 2009. Cannabinoid receptor 2 mediates the retention of immature B cells in bone marrow sinusoids. *Nat. Immunol.* 10:403–411. doi:10.1038/ni.1710

Pixley, F.J., and E.R. Stanley. 2004. CSF-1 regulation of the wandering macrophage: complexity in action. *Trends Cell Biol.* 14:628–638. doi:10.1016/j.tcb.2004.09.016

Plaks, V., T. Birnberg, T. Berkutzki, S. Sela, A. BenYashar, V. Kalchenko, G. Mor, E. Keshet, N. Dekel, M. Neeman, and S. Jung. 2008. Uterine DCs are crucial for decidua formation during embryo implantation in mice. *J. Clin. Invest.* 118:3954–3965.

Pollard, J.W., A. Bartocci, R. Arceci, A. Orlofsky, M.B. Ladner, and E.R. Stanley. 1987. Apparent role of the macrophage growth factor, CSF-1, in placental development. *Nature.* 330:484–486. doi:10.1038/330484a0

Pollard, J.W., J.S. Hunt, W. Wiktor-Jedrzejczak, and E.R. Stanley. 1991. A pregnancy defect in the osteopetrotic (op/op) mouse demonstrates the requirement for CSF-1 in female fertility. *Dev. Biol.* 148:273–283. doi:10.1016/0012-1606(91)90336-2

Redline, R.W. 2001. Macrophages in the basal plate of pre-eclamptic placentae. *Placenta.* 22:890–893. doi:10.1053/plac.2001.0726

Regenstreif, L.J., and J. Rossant. 1989. Expression of the c-fms proto-oncogene and of the cytokine, CSF-1, during mouse embryogenesis. *Dev. Biol.* 133:284–294. doi:10.1016/0012-1606(89)90319-9

Ryan, G.R., X.M. Dai, M.G. Dominguez, W. Tong, F. Chuan, O. Chisholm, R.G. Russell, J.W. Pollard, and E.R. Stanley. 2001. Rescue of the colony-stimulating factor 1 (CSF-1)-nullizygous mouse (Csf1(op)/Csf1(op)) phenotype with a CSF-1 transgene and identification of sites of local CSF-1 synthesis. *Blood.* 98:74–84. doi:10.1182/blood.V98.1.74

Sasmono, R.T., D. Oceandy, J.W. Pollard, W. Tong, P. Pavli, B.J. Wainwright, M.C. Ostrowski, S.R. Himes, and D.A. Hume. 2003. A macrophage colony-stimulating factor receptor-green fluorescent protein transgene is expressed throughout the mononuclear phagocyte system of the mouse. *Blood.* 101:1155–1163. doi:10.1182/blood-2002-02-0569

Schmid, M.A., D. Kingston, S. Boddupalli, and M.G. Manz. 2010. Instructive cytokine signals in dendritic cell lineage commitment. *Immunol. Rev.* 234:32–44. doi:10.1111/j.0105-2896.2009.00877.x

Schonkeren, D., M.L. van der Hoorn, P. Khedoe, G. Swings, E. van Beelen, F. Claas, C. van Kooten, E. de Heer, and S. Scherjon. 2011. Differential distribution and phenotype of decidual macrophages in preeclamptic versus control pregnancies. *Am. J. Pathol.* 178:709–717. doi:10.1016/j.ajpath.2010.10.011

Serbina, N.V., and E.G. Pamer. 2006. Monocyte emigration from bone marrow during bacterial infection requires signals mediated by chemokine receptor CCR2. *Nat. Immunol.* 7:311–317. doi:10.1038/ni1309

Shi, C., T. Jia, S. Mendez-Ferrer, T.M. Hohl, N.V. Serbina, L. Lipuma, I. Leiner, M.O. Li, P.S. Frenette, and E.G. Pamer. 2011. Bone marrow mesenchymal stem and progenitor cells induce monocyte emigration in response to circulating toll-like receptor ligands. *Immunity.* 34:590–601. doi:10.1016/j.immuni.2011.02.016

Stewart, I.J., and B.S. Mitchell. 1991. The distribution of uterine macrophages in virgin and early pregnant mice. *J. Anat.* 179:183–196.

Sudo, T., S. Nishikawa, M. Ogawa, H. Kataoka, N. Ohno, A. Izawa, S. Hayashi, and S. Nishikawa. 1995. Functional hierarchy of c-kit and c-fms in intramarrow production of CFU-M. *Oncogene.* 11:2469–2476.

Swirski, F.K., M. Nahrendorf, M. Etzrodt, M. Wildgruber, V. Cortez-Retamozo, P. Panizzi, J.L. Figueiredo, R.H. Kohler, A. Chudnovskiy, P. Waterman, et al. 2009. Identification of splenic reservoir monocytes and their deployment to inflammatory sites. *Science.* 325:612–616. doi:10.1126/science.1175202

Tsou, C.L., W. Peters, Y. Si, S. Slaymaker, A.M. Aslanian, S.P. Weisberg, M. Mack, and I.F. Charo. 2007. Critical roles for CCR2 and MCP-3 in monocyte mobilization from bone marrow and recruitment to inflammatory sites. *J. Clin. Invest.* 117:902–909. doi:10.1172/JCI29919

Tushinski, R.J., I.T. Oliver, L.J. Guilbert, P.W. Tynan, J.R. Warner, and E.R. Stanley. 1982. Survival of mononuclear phagocytes depends on a lineage-specific growth factor that the differentiated cells selectively destroy. *Cell.* 28:71–81. doi:10.1016/0092-8674(82)90376-2

van Furth, R. 1970. Origin and kinetics of monocytes and macrophages. *Semin. Hematol.* 7:125–141.

van Furth, R., and Z.A. Cohn. 1968. The origin and kinetics of mononuclear phagocytes. *J. Exp. Med.* 128:415–435. doi:10.1084/jem.128.3.415

Varol, C., L. Landsman, and S. Jung. 2009a. Probing in vivo origins of mononuclear phagocytes by conditional ablation and reconstitution. *Methods Mol. Biol.* 531:71–87. doi:10.1007/978-1-59745-396-7_6

Varol, C., A. Vallon-Eberhard, E. Elinav, T. Aychek, Y. Shapira, H. Luche, H.J. Fehling, W.D. Hardt, G. Shakhar, and S. Jung. 2009b. Intestinal lamina propria dendritic cell subsets have different origin and functions. *Immunity.* 31:502–512. doi:10.1016/j.immuni.2009.06.025

Varol, C., S. Yona, and S. Jung. 2009c. Origins and tissue-context-dependent fates of blood monocytes. *Immunol. Cell Biol.* 87:30–38. doi:10.1038/icb.2008.90

Wang, J.M., J.D. Griffin, A. Rambaldi, Z.G. Chen, and A. Mantovani. 1988. Induction of monocyte migration by recombinant macrophage colony-stimulating factor. *J. Immunol.* 141:575–579.

Welsh, A.O., and A.C. Enders. 1985. Light and electron microscopic examination of the mature decidual cells of the rat with emphasis on the antimesometrial decidua and its degeneration. *Am. J. Anat.* 172:1–29. doi:10.1002/aja.1001720102

Wiktor-Jedrzejczak, W., A. Bartocci, A.W. Ferrante Jr., A. Ahmed-Ansari, K.W. Sell, J.W. Pollard, and E.R. Stanley. 1990. Total absence of colony-stimulating factor 1 in the macrophage-deficient osteopetrotic (op/op) mouse. *Proc. Natl. Acad. Sci. USA.* 87:4828–4832. doi:10.1073/pnas.87.12.4828

Willman, C.L., C.C. Stewart, V. Miller, T.L. Yi, and T.B. Tomasi. 1989. Regulation of MHC class II gene expression in macrophages by hematopoietic colony-stimulating factors (CSF). Induction by granulocyte/macrophage CSF and inhibition by CSF-1. *J. Exp. Med.* 170:1559–1567. doi:10.1084/jem.170.5.1559

Wood, G.W., M. De, T. Sanford, and R. Choudhuri. 1992. Macrophage colony stimulating factor controls macrophage recruitment to the cycling mouse uterus. *Dev. Biol.* 152:336–343. doi:10.1016/0012-1606(92)90140-C